A Continuous-Wave Dye Laser for Raman Spectroscopy

by

James Kwan-Hung Chiu

Submitted in Partial Fulfillment
of the Requirements for the
Degree of Master of Science
at the
Oregon Graduate Center
July 1976

This Master's Thesis has been examined by the following committee of the Oregon Graduate Center:

Gail A. Massey
Professor, Dept

Lynwood W. Swanson
Professor, Dept. of Applied Physics and Electronic Science

Douglas F. Barofsky
Associate Professor,

TABLE OF CONTENTS

LIST OF FIGURES

1.0 INTRODUCTION

This monograph summarizes the theory and construction of a tunable continuous wave (CW) Rhodamine 6G dye laser longitudinally pumped by an argon laser. The CW dye laser efficiency and power output expressions derived from the intrinsic properties of a dye molecule are described in section 3.2. Section 3.3 contains the design of an astigmatic compensated 3-mirror resonator for the laser. The need for a flowing dye solution to improve dye laser efficiency and to prevent the dye solution from heating is discussed in section 3.4. From these basic considerations, the present system was designed and constructed using a flowing liquid cell or liquid jet for the laser medium, as described in section 4. Pilot experiments on the operation and properties of the dye laser were performed and are described in section 5.

2.0 LITERATURE SURVEY

In 1966, Sorokin and Lankard accidentally discovered that organic dye molecules can be used as a laser medium[1]. Intensive studies and experiments in the pulsed emission mode had been carried out by Weber and Bass[2], Pappalardo, et al[3], Snavely and Peterson[4], and Sorokin, et al[5,6]. Spectral narrowing and wavelength selectability from the wide fluorescence emission band of these molecules was shown possible by Soffer and McFarland in 1967 when they substituted a diffraction grating for one of the resonator mirrors[7]. Peterson, et al in 1970 announced

the first CW dye laser[8]. A recent, more efficient design employing a jet stream approach has been reported by Letouzey and Sari[9], Runge and Rosenberg[10], and Wellegehausen, et al[11]. Different dyes can now be employed to cover different parts of the whole visible spectrum[12].

3.0 THEORECTICAL CONSIDERATIONS

This section describes the general properties of dye molecules, from which the efficiency and power output of a flowing liquid laser using a dye solution as the active medium are derived through the coupled equations relating populations of the ground and excited states and the optical electromagnetic field intensity. From consideration of these expressions an estimate of the minimum pump power density required for lasing is made.

The resonator is designed to satisfy the required pump beam power density and such optical device parameters as tunability and astigmatic compensation of the dye cell arrangement. From the resonator design, the physical configuration of the lasing volume is specified to be a short cylinder with small cross-sectional area.

The need for a flowing dye solution to improve efficiency and remove the heat dissipated to the solvent from the high pump power density required is analysed.

3.1 PROPERTIES OF DYE MOLECULES

The following description of dye molecule properties follows closely that of Snavely[13].

An energy level diagram characteristic of an organic dye molecule is shown in Figure 1. The electronic ground state of the molecule is a singlet state, designated here as 1, which spans a range of energies determined by the quantized vibrational and rotational excitation of the molecule. The energy difference between vibrational states is typically of the order of 1400 to 1700 cm^{-1}. The energy spacing between rotational levels is smaller than the spacing between vibrational levels by a factor of approximately 100. The rotational levels, therefore, provide a near continuum of states between the vibrational levels.

Each excited electronic state of the molecule consists of a similar broad continuum, and optical transitions between these continua give rise to characteristic broad absorption and emission spectra as shown in Figure 2. The first and second excited singlet states are designated as 3 and 5 in Figure 1. Transitions between singlet states are selection-rule allowed, resulting in strong absorption and emission bands.

As the first step in the laser process, the molecules are excited from the lowest levels of the ground singlet 1 state to higher vibrational-rotational levels of the 3 state by absorbed light. This pro-

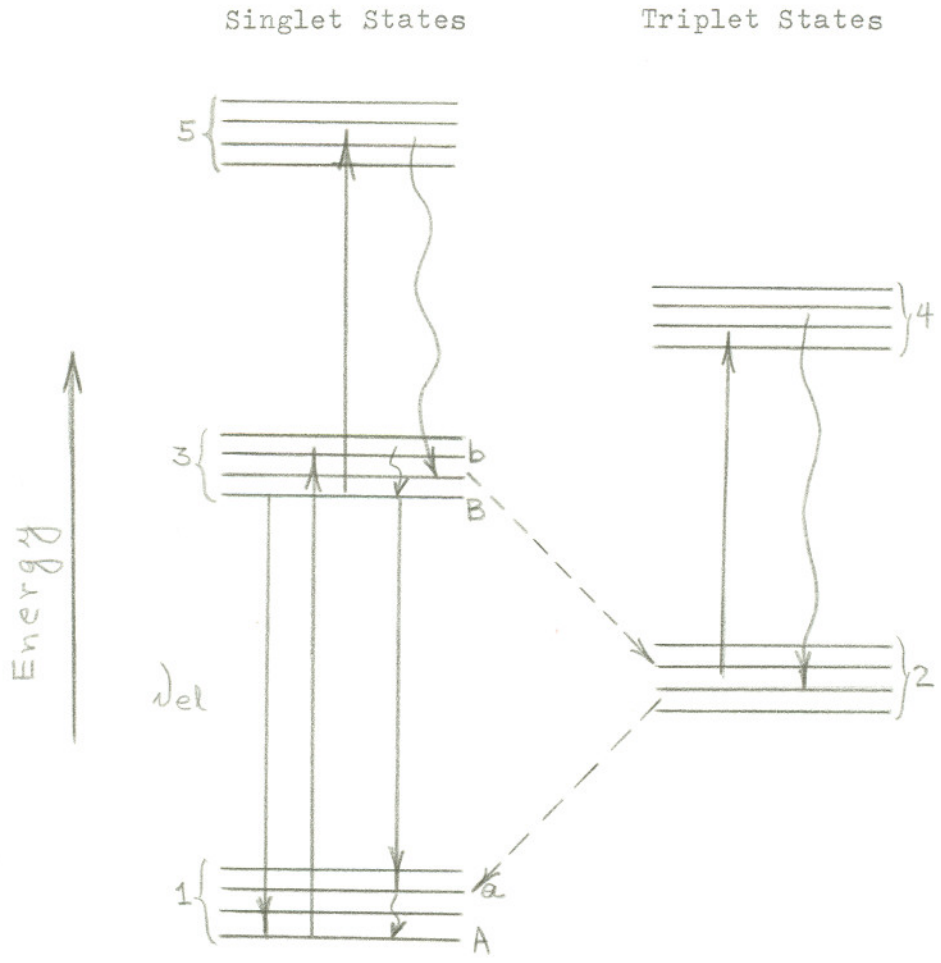

Figure 1 Schematic representation of the energy levels of a dye molecule[13]. The horizontal lines represent vibrational states. The solid lines are absorption and emission transitions. The wavy lines are radiationless transitions. The dotted lines are phosphorescence transitions.

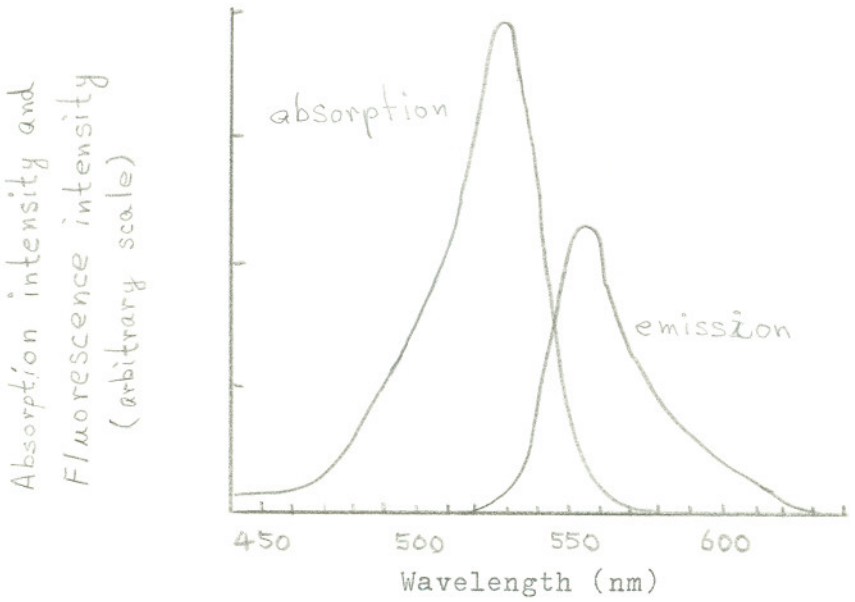

Figure 2 Absorption and fluorescence spectra of 10^{-4} molar solution of Rhodamine 6G in ethanol[13].

cess is indicated by the transition from state A to state b (A → b). The molecular energy then decays nonradiatively to level B, a low level of the 3 state, as indicated by the wavy line b → B. The laser emission results from the stimulated transition B → a. State a is a higher-lying vibrational-rotational state of 1. The laser process is terminated by the nonradiative decay a → A.

The particular transition from state A to state B is known as the (0, 0) transition frequency designated as ν_{el} in Figure 1.

The concentration of molecules in the excited singlet state 3 must reach a certain value, "the critical inversion", before coherent oscillation will be produced by the dye when placed in an optical

resonator. The magnitude of the critical inversion depends upon the losses of the complete laser system.

The decay of radiation emitted in the spontaneous singlet state process $B \rightarrow a$, known as fluorescence, is governed by the rate constant of state B. The rate constant k_{Ba} is the reciprocal of the exponential lifetime of a large number of dye molecules transiting from state B to state a.

The photon energy for which the optical absorption of the molecule is a maximum is greater than the photon energy at the fluorescence maximum. The energy difference between absorption and emission processes is taken up by the radiationless processes $b \rightarrow A$ and $a \rightarrow A$. The separation between fluorescence and singlet absorption spectra is important for the dye laser since the unexcited dye is transparent to the fluorescence radiation.

Molecules in the excited singlet 3 state may relax via a nonradiative process to a lower lying triplet state, designated as 2 in Figure 1, instead of decaying to the ground state. This process, known as intersystem crossing, proceeds at a rate governed by the intersystem crossing rate constant k_{32}. Intersystem crossing is indicated by a dashed line in Figure 1. Obviously intersystem crossing competes with fluorescence in the deactivation of 3. This competition is detrimental to the operation of the laser in several ways.

The rate constant for decay of the triplet state to the ground state, denoted by k_{21}, is generally much smaller than k_{31} since the triplet-singlet transition is selection-rule forbidden. The actual value of k_{21} depends upon experimental conditions. The decay process $2 \rightarrow 1$ may be radiative or nonradiative. The radiation accompanying the process is termed phosphorescence. Owing to its relatively small rate constant, k_{21}, the triplet state acts as a trap for the excited molecules and depletes the supply of molecules available for the laser process.

State 2 is the lowest-lying state of a manifold of excited triplet states, the first of which is indicated as 4 in Figure 1. Triplet-triplet transitions are selection-rule allowed and the optical absorption associated with these transitions is strong. Unfortunately, the corresponding absorption band generally overlaps the singlet-state fluorescence spectrum. Consequently, the accumulation of molecules in the triplet state produces a large optical loss at the wavelengths for which laser emission is probable. The absorption associated with triplet-triplet processes can be strong enough to quench or even prevent laser emission. In order to minimize the detrimental effects of the molecular triplet state, it is necessary to reach laser threshold before a significant number of molecules have accumulated in the triplet state. Because of this, all of the early dye laser experiments were performed in a pulse emission mode excited either by flashlamp[2], [3,4,5,13] or by ruby laser[6]. All of these studies required computer analysis of the coupled time-dependent differential equations, which

govern the population of the states.

The triplet state of many dye molecules is highly reactive chemically. Thus, the relaxation of the triplet to singlet ground state may be enhanced through the use of chemical additives, known as triplet quenchers, e.g. oxygen[13], Ammonyx-LO[14,15], Triton-X100[8], and cyclo-octatetraene[3]. The value of k_{21} has been reported to vary from 10^7 $second^{-1}$ in an oxygen saturated alcohol solution to 10^3 $second^{-1}$ or less in a carefully degassed dye solution. A substantial improvement in dye laser performance has been shown with the addition of triplet quencher in the dye solution. This improvement can be traced to the higher relaxation rate of the triplet state to the singlet ground state.

Optical absorption between excited singlet states, such as the process connecting 3 and 5 in Figure 1, is also a possible source of optical loss in the dye laser. The importance of this process is difficult to assess at this time. This optical loss is probably not as serious as that associated with the triplet-triplet transitions, since the population of the 3 state remains relatively small when compared to that of the 1 or 2 state.

3.2 KINETICS OF LASING VOLUME

The laser action and performance of a CW dye laser may be best

understood through a careful study of the active region. The theoretical efficiency and power output can be calculated by meticulously accounting for each and every process that occurs within the lasing volume. For the present work on a CW laser, the steady state solutions are obtained by setting the various rate equations equal to zero.

First assume that a set of four electronic vibrationally broadened levels (two singlets and two triplets), are sufficient to account for the kinetics of the laser. Figure 1 can then be simplified to that of figure 3. With this assumption, there are only two decay paths for the state 3: fluorescence and intersystem crossing. The singlet-triplet rate constant k_{32} can now be estimated through the definition of quantum yield ϕ[13,16].

$$\phi = \frac{\text{number of fluorescence photons emitted per second}}{\text{number of excitation photons absorbed per second}} \qquad 1$$

$$\text{or,} \quad \frac{1-\phi}{\phi} = \frac{\text{number of excited molecules decaying other than by fluorescence per second}}{\text{number of fluorescence photons emitted per second}} \qquad 2$$

By associating the number of fluorescence photons emitted per second with the decay rate constant for the singlet-singlet transition k_{31}, and the balance of the excited molecules decaying other than by fluorescence per second with the intersystem decay rate constant k_{32}, eq. 2 can then be expressed as

$$k_{32} = \frac{1-\phi}{\phi} k_{31} \qquad 3$$

where k_{ij} = reciprocal of the exponential transition lifetime of a large number of excited dye molecules in state i to state j.

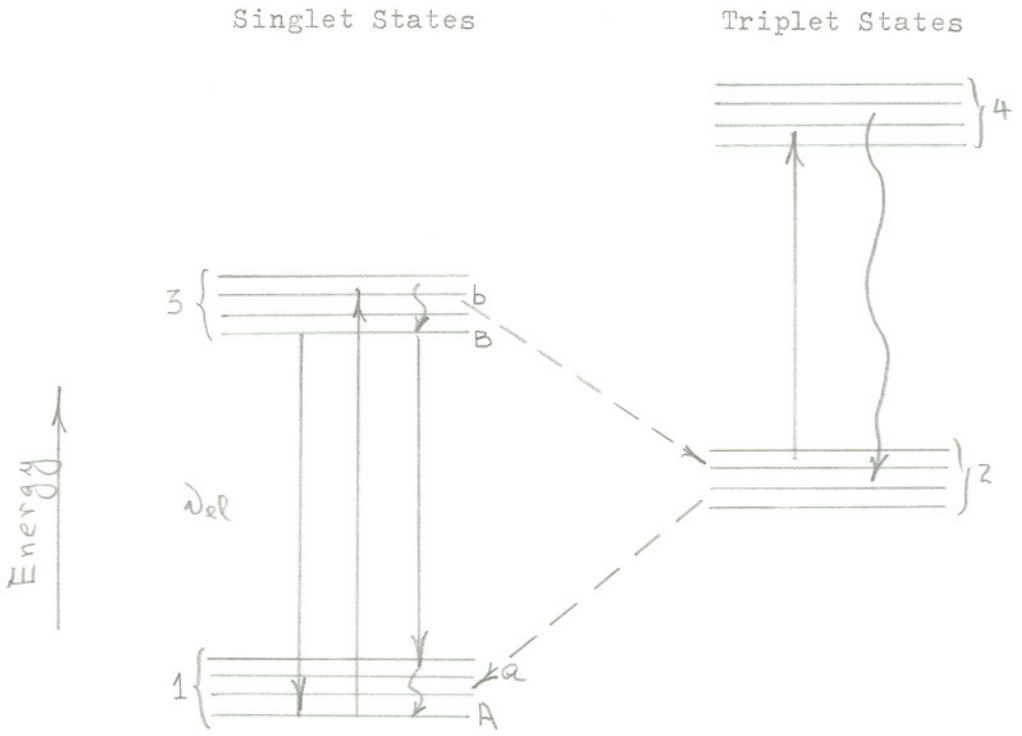

Figure 3 Simplified schematic representation of the energy levels of a dye molecule. The horizontal lines represent vibrational states. The solid lines are absorption and emission transitions. The wavy lines are radiationless transitions. The dotted lines are phosphorescence transitions.

This expression tends to over estimate the intersystem crossing rate constant. This over estimation, however, does not seriously affect the analysis[15].

Secondly, it is assumed that the decay rate constant of the excited triplet state is greater than the excitation rate constant; in other words,

$$k_{42} >> k_{24}, \qquad 4$$

the population density of the excited triplet state 4 can be ignored. Under this assumption, the triplet accumulation from state 3 due to intersystem decay is balanced only by the triplet state 2 depopulation to the singlet ground state 1. The triplet equation constituting the first simultaneous equation can now be written.

$$k_{32}\, n_3 = k_{21}\, n_2 \qquad 5$$

The second simultaneous equation relates the dye molecule conservation and the fraction of light absorbed, f.

$$f \equiv 1 - \exp\left(-\left(n_1 + n_2 + n_3\right) \sigma_p\, l\right) \qquad 6$$

where n_i = population density of the i^{th} electronic state (molecules/cm^3),

σ_p = absorption cross section at pump frequency (cm^2), and

l = length of active region (cm).

A third simultaneous equation is needed to find the three coupled population densities of state 1, 2 and 3. This relationship can be derived by considering the optical electromagnetic field intensity within the active region. The growth of intensity in a laser mode as a result of amplification by the active medium can be described as

$$\frac{d\, I_L}{d\, z} = G\, I_L \qquad 7$$

where I_L = intracavity dye laser flux density (Watt/cm^2),

$d\, z$ = displacement in the direction of propagation (cm), and

G = net effective gain coefficient of the medium and the resonator structure.

By assuming that the gain coefficient of the dye laser is uniform within the lasing volume, G is then the difference between the gain by stimulated emission $3 \rightarrow 1$ and the losses by the self absorption $1 \rightarrow 3$, triplet-triplet absorption $2 \rightarrow 4$, diffraction and scattering losses at various surfaces (e.g. mirrors, glass, etc.), and loss due to output mirror transmissivity. Under the steady state conditions, G is set equal to zero.

$$G = 2\sigma_{31}(\nu_L) n_3 l - 2\sigma_{13}(\nu_L) n_1 l - 2\sigma_{24}(\nu_L) n_2 l - S - T = 0 \qquad 8$$

where $\sigma_{ij}(\nu_a)$ = absorption or emission cross section from state i to state j at frequency ν_a (cm^2),

ν_L = dye laser emission frequency (Hz),

S = fractional loss per pass including diffraction, scattering, etc. at various surfaces ($S \ll 1$), and

T = output mirror transmissivity ($T \ll 1$).

The above cross sections are effective (per molecule) values as averages over the absorption or emission band population differences.

Due to the Stokes shift between emission and absorption bands, the cross sections $\sigma_{31}(\nu_L)$ and $\sigma_{13}(\nu_L)$ are not equal, as is the case for sharp levels, but are related through Boltzmann's distribution.

Stepanov and Rubinov[17], by assuming that the probabilities of redistribution of the electrons over the sublevels of 1 and 3 are considerably greater than the probabilities of optical and nonoptical transitions between the vibrational states, proved that

$$\sigma_{31}(\nu_L) = \sigma_{13}(\nu_L)\beta \qquad 9$$

where $\beta = \exp\left(\frac{h(\nu_{el} - \nu_L)}{kT_o}\right)$,

ν_{el} = (0,0) transition frequency (Hz),

k = Boltzmann constant, and

To = temperature of dye molecule (°K).

By solving the simultaneous equations 5, 6 and 8, the population density of each state can be obtained as

$$n_1 = \frac{1}{D\ell}\left[N(\sigma_{31}(\nu_L)k_{21} - \sigma_{24}(\nu_L)k_{32}) - \alpha(k_{32} + k_{21})\right] \qquad 10$$

$$n_2 = \frac{1}{D\ell}\left[\alpha + N\sigma_{13}(\nu_L)\right]k_{32} \qquad 11$$

$$n_3 = \frac{1}{D\ell}\left[\alpha + N\sigma_{13}(\nu_L)\right]k_{21} \qquad 12$$

where $D = \sigma_{31}(\nu_L)k_{21} + \sigma_{13}(\nu_L)k_{32} + \sigma_{13}(\nu_L)k_{21} - \sigma_{24}(\nu_L)k_{32}$

$\alpha = \frac{S+I}{2}$

$N = \frac{1}{\sigma_p}\ln\left(\frac{1}{1-f}\right)$

The steady state excited singlet state equation can be written as

$$\frac{P_{in}}{h\nu_p}\frac{f}{V_p}\frac{n_1}{n_1+n_2+n_3} + \frac{I_L}{h\nu_L}\sigma_{13}(\nu_L)n_1 = \frac{I_L}{h\nu_L}\sigma_{31}(\nu_L)n_3 + k_{32}n_3 \qquad 13$$

where P_{in} = constant pump power (Watt),

V_p = volume of uniformly pumped region (cm^3), and

h = Planck constant.

The $h\nu_L$ and $h\nu_p$ are quantum energies at the emission and pumping frequencies. The first and second terms correspond to excitation of state $1 \rightarrow 3$ by fractional absorption of another CW laser light with constant pump power P_{in} at a discrete frequency ν_p and reabsorption of emitted dye laser light respectively, whereas the third and fourth terms correspond to the excited singlet state depopulation by stimulated emission and depopulation via the triplet state respectively. By substituting eq. 10 and eq. 12 into eq. 13, the intracavity dye laser flux density can be shown to be

$$I_L = \frac{\nu_L}{\nu_p} \frac{f}{v_p} \frac{\ell}{N} \frac{\gamma}{\frac{\alpha}{N}\left(\frac{\sigma_{31}(\nu_L)}{k_{32}} + \frac{\sigma_{13}(\nu_L)}{k_{21}} + \frac{\sigma_{13}(\nu_L)}{k_{32}}\right) + \frac{\sigma_{13}(\nu_L)\sigma_{24}(\nu_L)}{k_{21}}} \left[P_{in} - \frac{h\nu_p}{\ell} \frac{v_p}{f} \frac{\alpha + N\sigma_{13}(\nu_L)}{\gamma}\right] \quad 14$$

where $$\gamma = \frac{\sigma_{31}(\nu_L)}{k_{32}} - \frac{\sigma_{24}(\nu_L)}{k_{21}} - \frac{\alpha}{N}\left(\frac{1}{k_{21}} + \frac{1}{k_{32}}\right)$$

As half of the dye laser flux I_L is moving in one direction within the resonator, the laser power output through the output mirror can be immediately written as

$$P_{out} = \frac{1}{2} I_L TA \quad 15$$

where P_{out} = dye laser power output (Watt), and

A = cross-sectional area of active volume (cm^2).

Putting eq. 14 into eq. 15, it is evident that

$$P_{out} = \frac{T}{2} \frac{\nu_L}{\nu_p} \frac{v_L}{v_p} \frac{f}{N} \frac{\gamma}{\frac{\alpha}{N}\left(\frac{\sigma_{31}(\nu_L)}{k_{32}} + \frac{\sigma_{13}(\nu_L)}{k_{21}} + \frac{\sigma_{13}(\nu_L)}{k_{32}}\right) + \frac{\sigma_{13}(\nu_L)\sigma_{24}(\nu_L)}{k_{21}}} \left[P_{in} - \frac{h\nu_p}{f} \frac{v_p}{v_L} \frac{\alpha + N\sigma_{13}(\nu_L)}{\gamma} A\right] \quad 16$$

By inspection of eq. 16, it is obvious that P_{out} has a linear dependence on the pump power P_{in}. It is then natural to define a slope

efficiency $\eta = \frac{\partial P_{out}}{\partial P_{in}}$. By substituting eq. 3 and eq. 9 into eq. 16, η can be identified.

$$\eta = \frac{T}{2}\frac{\nu_L}{\nu_p}\frac{V_L}{V_p}\frac{f}{\ln\left(\frac{1}{1-f}\right)}\sigma_p \frac{\frac{\phi}{1-\phi}\frac{\sigma_{13}(\nu_L)}{k_{31}}\beta - \frac{\sigma_{24}(\nu_L)}{k_{21}} - \frac{S+T}{2}\frac{\sigma_p}{\ln\left(\frac{1}{1-f}\right)}\left[\frac{1}{k_{21}} + \frac{\phi}{1-\phi}\frac{1}{k_{31}}\right]}{\frac{S+T}{2}\frac{\sigma_p}{\ln\left(\frac{1}{1-f}\right)}\sigma_{13}(\nu_L)\left[\frac{\phi}{1-\phi}\frac{\beta}{k_{31}} + \frac{\phi}{1-\phi}\frac{1}{k_{31}} + \frac{1}{k_{21}}\right] + \frac{\sigma_{13}(\nu_L)\sigma_{24}(\nu_L)}{k_{21}}} \qquad 17$$

Further examination of eq. 16 reveals that P_{in} has to overcome an inherent power requirement before there is any dye laser oscillation. This requirement can be identified as the threshold power density I_T. Thus, after substituting eq. 3 and eq. 9 into eq. 16, the threshold power density I_T can be defined as

$$I_T = \frac{h\nu_p}{f}\frac{V_p}{V_L}\frac{\frac{S+T}{2} + \frac{\sigma_{13}(\nu_L)}{\sigma_p}\ln\left(\frac{1}{1-f}\right)}{\frac{\phi}{1-\phi}\frac{\sigma_{13}(\nu_L)}{k_{31}}\beta - \frac{\sigma_{24}(\nu_L)}{k_{21}} - \frac{S+T}{2}\frac{\sigma_p}{\ln\left(\frac{1}{1-f}\right)}\left(\frac{1}{k_{21}} + \frac{\phi}{1-\phi}\frac{1}{k_{31}}\right)} \qquad 18$$

where I_T = threshold power density (Watt/cm^2)

Because the threshold power density I_T must be reached before there is any dye laser oscillation, it is important to estimate this threshold requirement. For the present work on a Rhodamine 6G dye laser, the typical values of dye laser parameters are given in Table 1.

Table 1. TYPICAL VALUES OF DYE LASER PARAMETERS (Rhodamine 6G)[13,15]

ϕ	= 0.85	
σ_{13} (580 nm)	= 2.67 x 10^{-18}	cm^2
σ_{24}(580 nm)	= 3.66 x 10^{-17}	cm^2
σ_p	= 2.105 x 10^{-16}	cm^2
k_{31}	= 1.35 x 10^{8}	sec.$^{-1}$

$$\nu_{el} = 5.4549 \times 10^{14} \text{ Hz}$$

$$\nu_{p} = 5.8309 \times 10^{14} \text{ Hz}$$

$$\beta\ (273\ ^{\circ}\text{K},\ 580\ \text{nm}) = 1.1792 \times 10^{2}$$

$$S \sim 0.01$$

$$f \sim 0.9$$

As was pointed out in section 3.1, the triplet-singlet transition rate constant k_{21} varies depending on experimental conditions, and it is necessary to know k_{21} in order to calculate the threshold power density I_T. For the present, if it is assumed that the dye laser mode volume V_L matches exactly with the pump beam mode volume V_p, or $V_L / V_P \sim 1$, I_T can be calculated by substituting the dye laser parameters into eq. 18. I_T is plotted as a function of k_{21} with the output mirror transmissitivity T as a variable parameter as shown in Figure 4.

It can be seen from figure 4 or by inspection of eq. 18 that even if T = 0, k_{21} still has to be greater than 2.80×10^{6} sec.$^{-1}$ before the dye laser oscillates. Furthermore, I_T approaches a minimum value of 1.12 kW/cm^2 if the triplet-singlet decay rate constant k_{21} has the same magnitude as the singlet-triplet decay rate constant k_{32}. k_{32} is given by eq. 3 to be $\frac{1-\phi}{\phi} k_{31}$. Thus, it is obvious from figure 4 that I_T can vary between 1.12 kW/cm^2 and infinity depending on the value of k_{21}. The detrimental effect of triplet state accumulation due to a low triplet-singlet transition is at once evident.

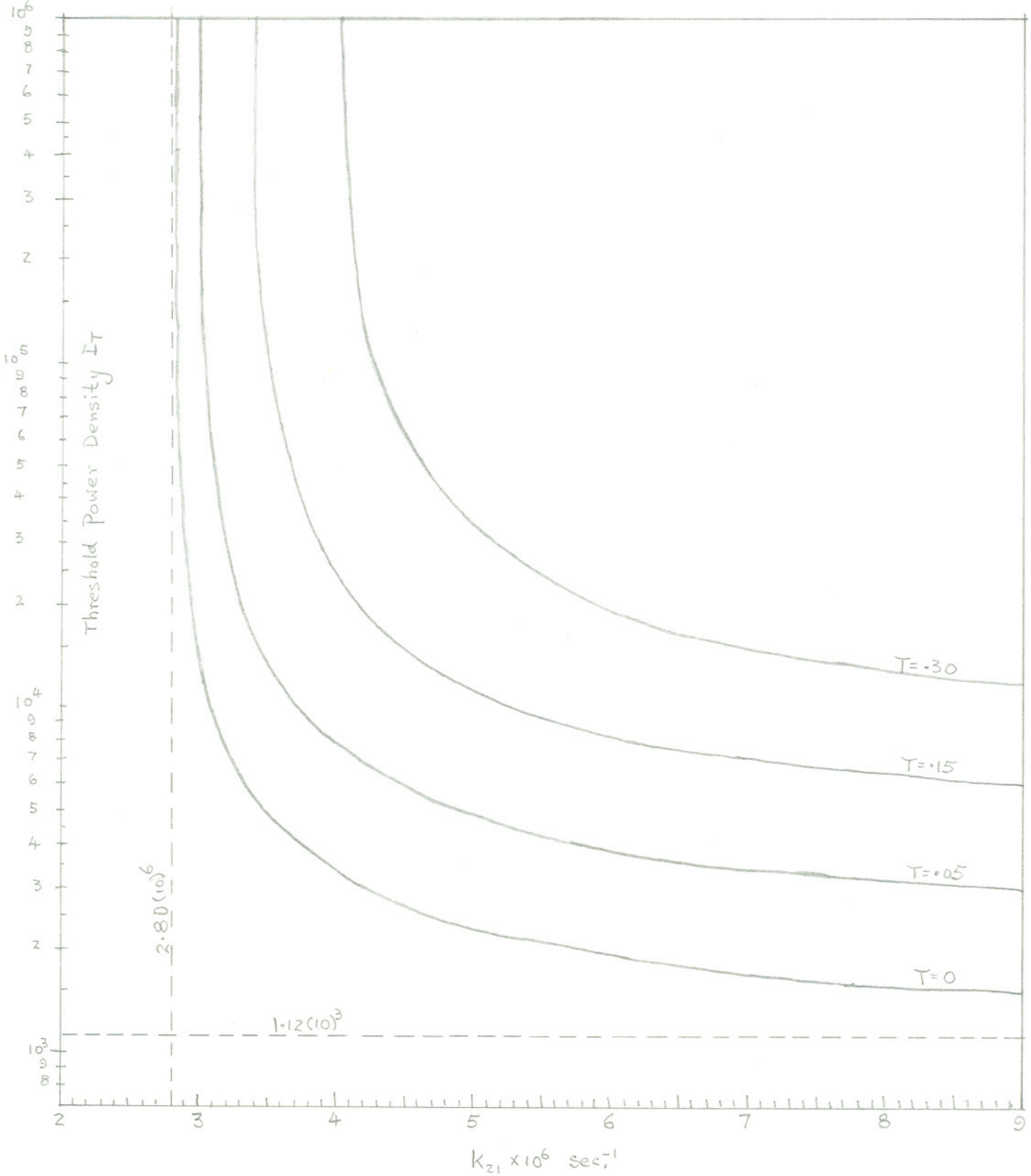

Figure 4 Threshold power density I_T vs triplet-singlet decay rate constant

Similarly, the dye laser efficiency is plotted as a function of k_{21} with T as a variable parameter in figure 5. The increase in efficiency due to an increase in the triplet-singlet transition is again obvious. It is also obvious that the optimum output mirror transmissivity is about 15%. If the triplet-singlet decay is as fast as the singlet-triplet, or $k_{21} = k_{32}$, a slope efficiency of 63.1% can be predicted.

3.3.0 RESONATOR ANALYSIS

The previous section discussed the kinetics of the gain region, but a laser oscillator is not complete without a resonator to provide both storage and feedback. Section 3.3.1 discusses the necessity of a 3-mirror folded resonator and the compensation analysis for the astigmatism introduced by certain optical members of the cavity. The resonator is then designed to meet the pump power density requirement and satisfy the wave propagation properties. By the characteristic of wave propagation, the physical dimension of the lasing region is specified to be a short cylindrical rod with small cross-sectional area. Lastly, the output linewidth of the dye laser is derived from the dispersion property of the prism.

3.3.1 ASTIGMATIC COMPENSATION OF A 3-MIRROR FOLDED RESONATOR

The active section consists of a flowing film of organic dye solu-

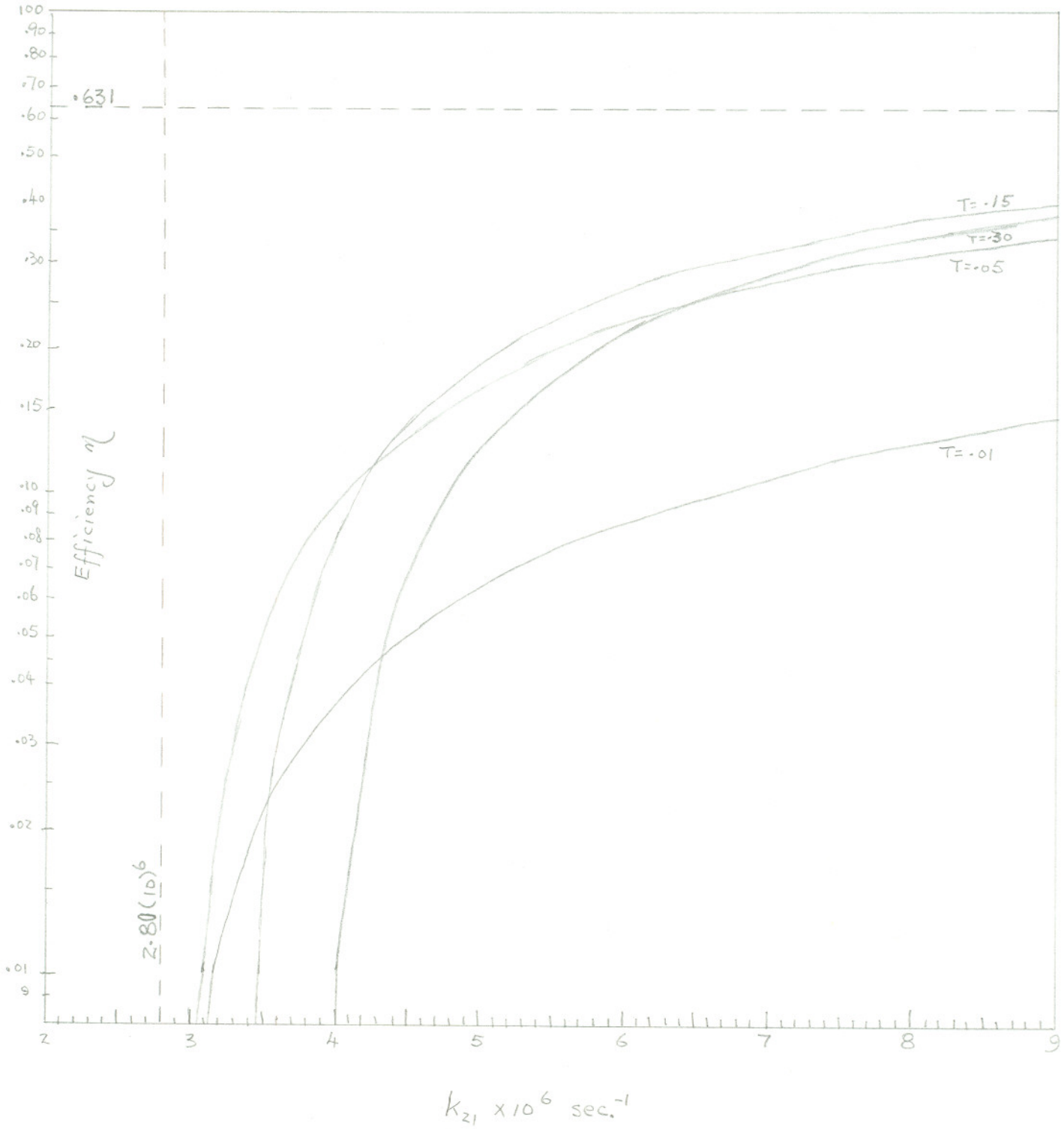

Figure 5 Laser efficiency vs triplet-singlet decay rate constant

tion either confined within a cell with windows or projected through open space by a nozzle within the resonator. Both of these approaches have been attempted and are discussed later.

To minimize losses due to surface reflection, the "sheet" of fluid is either positioned at the Brewster angle or the windows used in the cell are anti-reflection (AR) coated and positioned at normal incidence. Due to the high cost and optical damage susceptibility of AR coatings, the experiments were performed with the "sheet" oriented at the Brewster angle.

A parallel plate introduces astigmatism when positioned at an angle to the light beam. Thus, in order to obtain a laser mode with low diffraction losses, the optical defect must be compensated.

Figure 6 shows a parallel plate of thickness t_s and a refractive index n_s, with a light beam incident at the Brewster angle, i.e. $\theta_s = \arctan(n_s)$. By using the refraction ray matrices across a boundary obtained by matching the transverse phase and amplitude variations of the incident, reflected and refracted waves[18], it can be shown that the effective

$$\text{sagittal distance} \quad (xz \text{ plane}) = S_s = \frac{t_s}{n_s^2}\left[1+n_s^2\right]^{\frac{1}{2}}, \qquad 19$$

and

$$\text{tangential distance} \quad (yz \text{ plane}) = T_s = \frac{t_s}{n_s^4}\left[1+n_s^2\right]^{\frac{1}{2}}. \qquad 20$$

The difference between the sagittal distance and tangential distance is then

$$\Delta S = S_S - T_S = \frac{t_S}{n_S^4}(n_S^2 - 1)(1 + n_S^2)^{\frac{1}{2}}$$

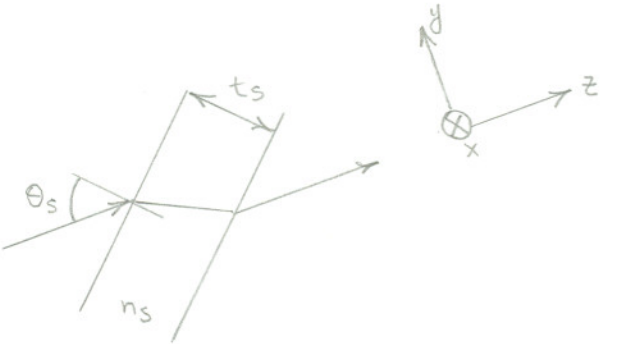

Figure 6 Parallel plate at Brewster angle

For example, if the plate is a parallel "sheet" of ethylene glycol with refractive index 1.43 and a thickness of 0.25 mm, ΔS can be calculated to be 0.109 mm. For an enclosed cell consisting of three parallel "plates", two of them glass of thickness 1.60 mm and refractive index 1.53 sandwiching a "sheet" of ethanol of thickness 1 mm and refractive index 1.329, it can be shown that the total

$$\Delta S = 2 \times \Delta S_{glass} + \Delta S_{ethanol} = 1.65 \text{ mm}.$$

Furthermore, if the laser is to be wavelength tunable, selective losses must be used to discriminate against some of the free running frequency modes. A number of schemes have been employed, such as diffraction gratings[7] or Pockels cells[19]. A Brewster dispersive prism was used in the present design because it has lower optical insertion loss than the diffraction grating or the Pockels cell. The output linewidth obtained with a prism is sufficiently narrow to be

useful as a light source for Raman spectroscopy. However, the prism also introduces a small additional astigmatism but it is always set at such a position that the difference in pathlengths is not critical and can be neglected as shown in the next section.

Another optical element that can introduce astigmatism is a mirror used at oblique incidence. The mirror then focuses the sagittal (xz) ray bundles at a different location than the tangential (yz) bundles. This is reflected in two different focal lengths f_x and f_y, which are related to the normal incidence focal length f of the mirror by[20]

$$f_x = \frac{f}{\cos(\phi)} \qquad 22$$

and

$$f_y = f \cos(\phi) \qquad 23$$

where ϕ is the angle of incidence of the ray bundle axis on the mirror.

With these optical defects, it is possible to offset one with another to cause the focal points in the xz and yz planes to coincide. By requiring that

$$f_x - f_y = \Delta S$$

and substituting $f = \frac{R}{2}$ yields

$$\sin(\phi)\tan(\phi) = \frac{2}{R}\Delta S \qquad 24$$

where R = radius of curvature of the mirror.

For example, a mirror with radius of curvature 10 cm, the compensation angle for the parallel "sheet" of ethylene glycol can be cal-

culated to be 2.67°. And with the same mirror, the compensation angle for the three parallel "sheets": glass-ethanol-glass can be calculated to be 10.37°.

With the astigmatic compensation expected by setting one of the resonator mirrors at an angle to the dye laser beam, the arrangement of the resonator components is at once evident. As shown in figure 8, the mirror R_3 is set at an angle ϕ to the normal incidence of the dye laser beam. Because R_3 is set at an angle, a third mirror R_2 is needed to 'cap' the resonator - to contain the dye laser irradiance within the resonator. The solid line in figure 8 indicates the resonator optic axis.

As is shown in figure 8, a pump beam P_{in} can be brought into the resonator in two possible ways. P_{in} can be introduced directly into the mirror R_3 as in figure 8a. Alternatively, P_{in} can be brought in through the Brewster prism as in figure 8b. It is possible to introduce P_{in} into the resonator through the prism because the angle of deviation is different for light with different wavelengths.

3.3.2 3-MIRROR FOLDED RESONATOR ANALYSIS

In the discussion of section 3.2, it was demonstrated that high pump power density ($> 10^3$ Watt/cm^2) is required at the lasing region. Since a useful laser oscillator must operate well above threshold, a

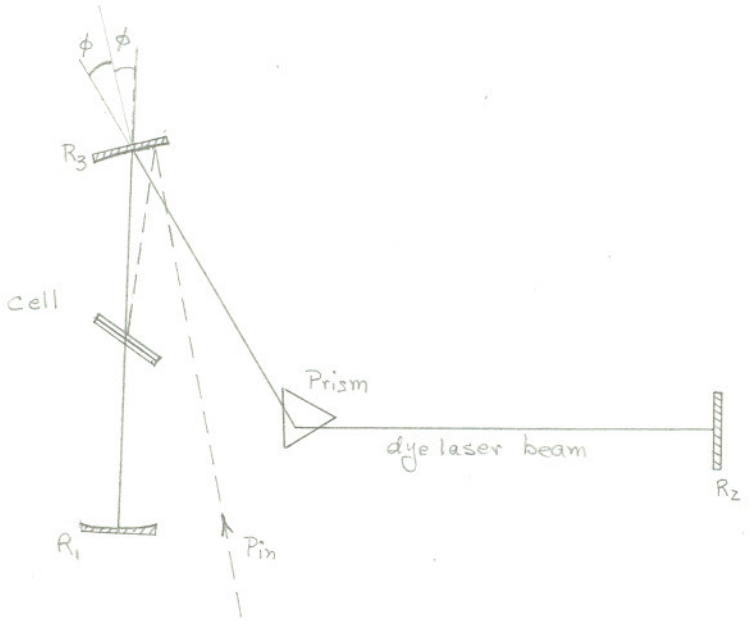

(a)

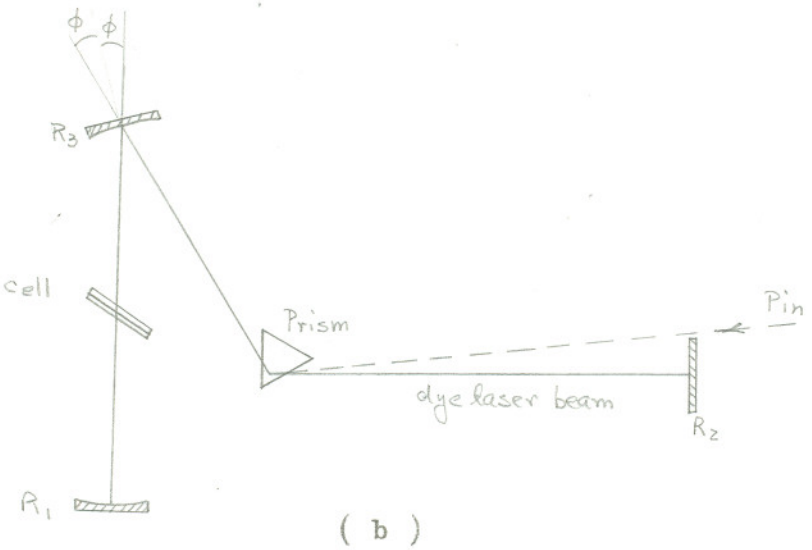

(b)

Figure 8 Different experimental configurations
R_1, R_2, R_3 are mirrors

more realistic power density is about 10 kWatt/cm^2.

The power density is inversely proportional to the beam cross-sectional area as shown in figure 9. The graph is drawn by assuming that 63.2% of light intensity is contained within one beam radius. It shows that if 10 kW/cm^2 of power density is to be achieved, the beam radius must be $\lesssim$ 0.025 mm. With 10 kW/cm^2 of pump power and if the triplet-singlet decay rate constant is greater than 3×10^6 $sec.^{-1}$, laser oscillation should be achieved.

The desired beam cross-sectional area can be achieved by properly focusing the incoming pump beam. This focusing can be accomplished by a spherical mirror or a lens. An ideal thin lens of focal length f transforms an incoming spherical wave with radius R_1 immediately to the left of the lens into a spherical wave with radius R_2 immediately to the right of it, as shown in figure 10, where[21]

$$\frac{1}{R_2} = \frac{1}{R_1} - \frac{1}{f} \qquad 25$$

The radius of curvature is taken to be positive if the wavefront is convex as viewed from $z = \infty$.

The phase front radius of the pump laser beam in our case is nearly infinite, viz, the wave front of the laser beam is plane. Thus R_1 is ∞ and eq. 25 reduces to

$$\frac{1}{R_2} = -\frac{1}{f} \qquad 26$$

For the case of concave spherical mirror the focal length $f = \frac{R_m}{2}$ where

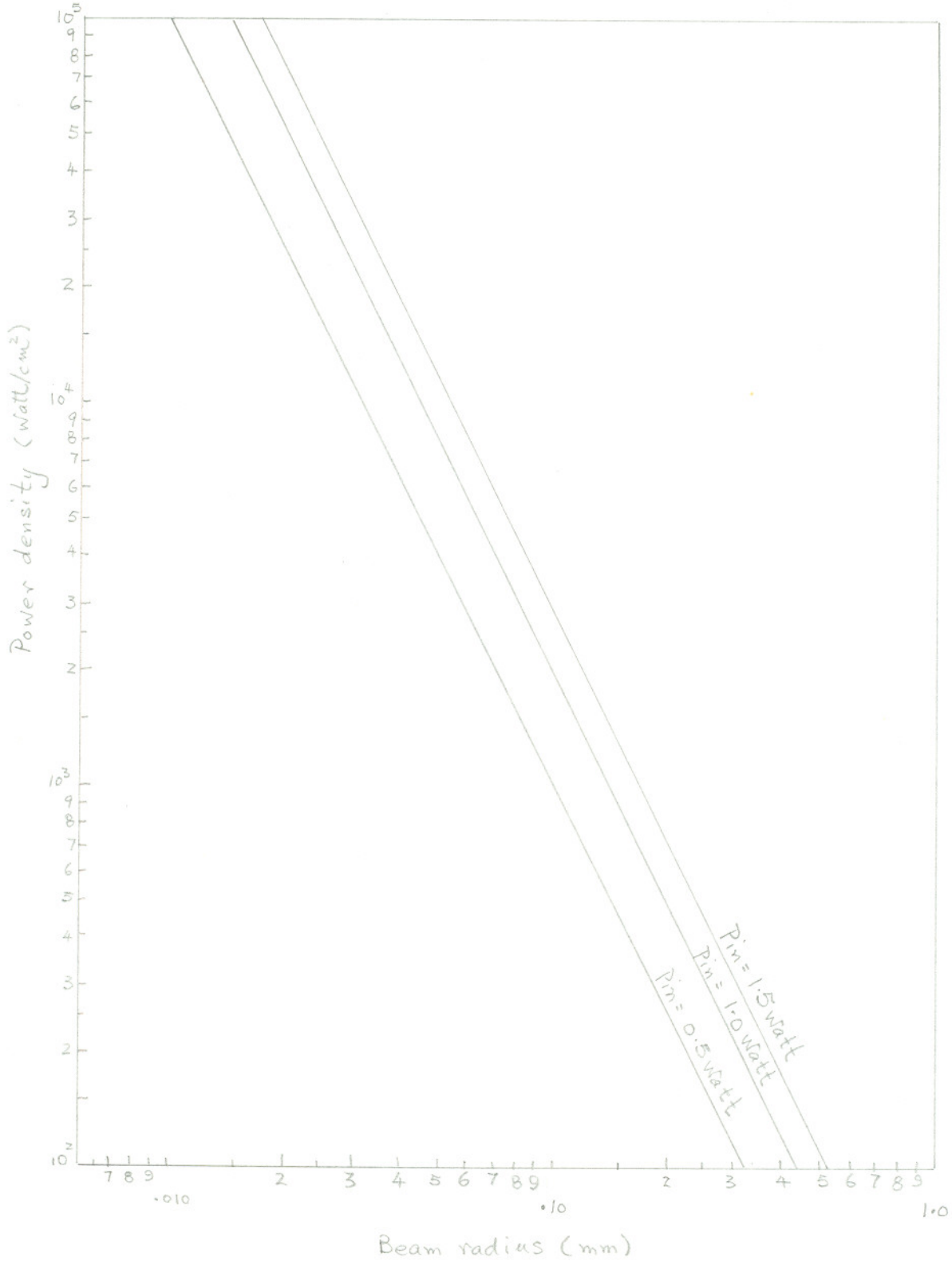

Figure 9 Power density vs beam radius

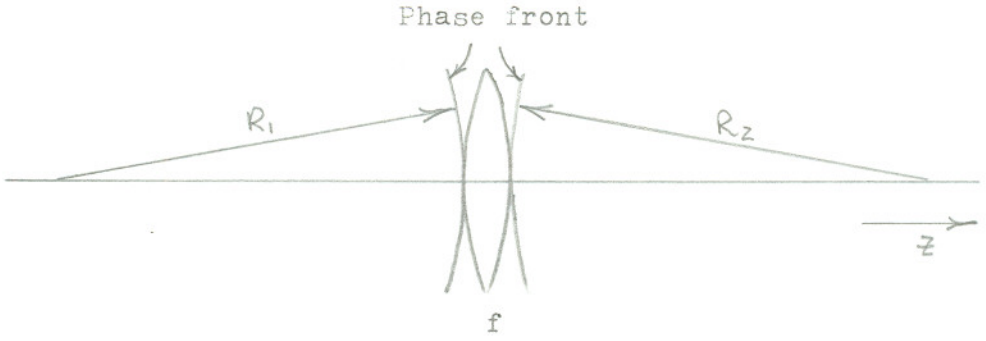

Figure 10 Transformation of wavefront by a thin lens

R_m is the radius of curvature of the mirror, thus

$$\frac{1}{R_2} = \frac{2}{R_m} \qquad 27$$

The transformed spherical wave then propagates towards the dye cell region. By assuming a slowly varying complex intensity distribution perpendicular to the propagation axis and using the scalar wave equation, it can be shown that the transverse beam amplitude function remains Gaussian if the input plane wave is Gaussian[21,22], which is the case for the pump laser used in these experiments. By introducing two real beam parameters in the complex parameter

$$\frac{1}{q} = \frac{1}{R} - j\frac{\lambda}{\pi\omega^2}$$

where R = radius of curvature of the phase front, and λ = beam wavelength, and utilizing the properties derived from the wave equation, it can be shown that the beam radius propagates along the z axis according to the relation[21,22] (see figure 11)

$$\omega^2(z) = \omega_0^2\left[1 + \left(\frac{\lambda z}{\pi\omega_0^2}\right)^2\right] \qquad 28$$

and the wave front curvature R is

$$R(z) = z\left[1+\left(\frac{\pi\omega_o^2}{\lambda z}\right)^2\right] \qquad 29$$

where ω = radius where the beam intensity is 1/e that on the axis,

ω_o = beam waist radius where the phase front is plane, and

z = distance measured from the beam waist.

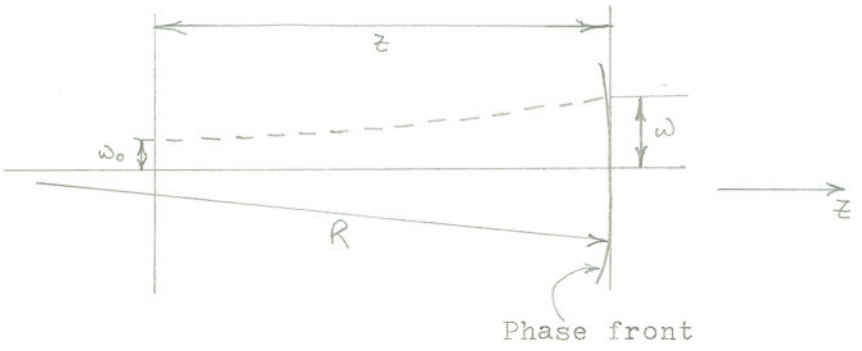

Figure 11 Contour of a Gaussian Beam

By solving eq. 28 and eq. 29 simultaneously, it can be shown that

$$\omega_o^2 = \omega^2\left[1+\left(\frac{\omega^2\pi}{R\lambda}\right)^2\right]^{-1}, \qquad 30$$

and

$$z = R\left[1+\left(\frac{R\lambda}{\omega^2\pi}\right)^2\right]^{-1}. \qquad 31$$

If the same 10 cm radius mirror that was selected in our compensation calculation is used to focus the 1 watt argon laser beam which has a wavelength of 514.5 nm and beam waist of 0.34 mm, by employing eq. 27, eq. 30 and eq.31, it can be shown that a 'spot' radius of 0.024 mm can be produced at a distance of about 5 cm from, or at the focus of, the spherical mirror. With the beam radius transformed to 0.024 mm, the power density from the 1 watt argon laser can then be expected to

be about 3.49×10^4 watt/cm^2. This is then a substantial amount above the minimum threshold power density of 1.12 kW/cm^2.

Further examination of eq. 28 reveals that the beam radius expands as a function of wavelength and distance from the beam waist. For optimum dye laser efficiency, it is necessary to have the dye laser beam mode volume contained within the pump beam mode volume.

The mode volume of a 'cylindrical' beam can be calculated using eq. 28 as

$$V = \int_{-\frac{t_s}{2}}^{\frac{t_s}{2}} \pi \omega_o^2 \left[1 + \left(\frac{\lambda x}{\pi \omega_o^2}\right)^2\right] dx \qquad 32$$

where V = mode volume, and

t_s = length of 'cylindrical' rod.

By using eq. 32, the ratio of the mode volume difference between the dye laser beam V_L and the pump beam V_P to the pump beam volume V_P can be formed.

$$\frac{V_L - V_P}{V_P} = \frac{\frac{1}{3}\left(\frac{t_s}{2\pi\omega_o^2}\right)^2 \left[\lambda_L^2 - \lambda_P^2\right]}{1 + \frac{\lambda_P^2}{3}\left(\frac{t_s}{2\pi\omega_o^2}\right)^2} \qquad 33$$

where

λ_P = pump wavelength = 514.5 nm, and

λ_L = dye laser wavelength.

A graph of eq. 33 is plotted in figure 12 as function of cell thickness t_s and variable parameter λ_L. It is obvious that to have low loss and wide tunability, t_s must be small. A maximum cell thickness of 1 mm, would mean an 'overlap' of 0.2%

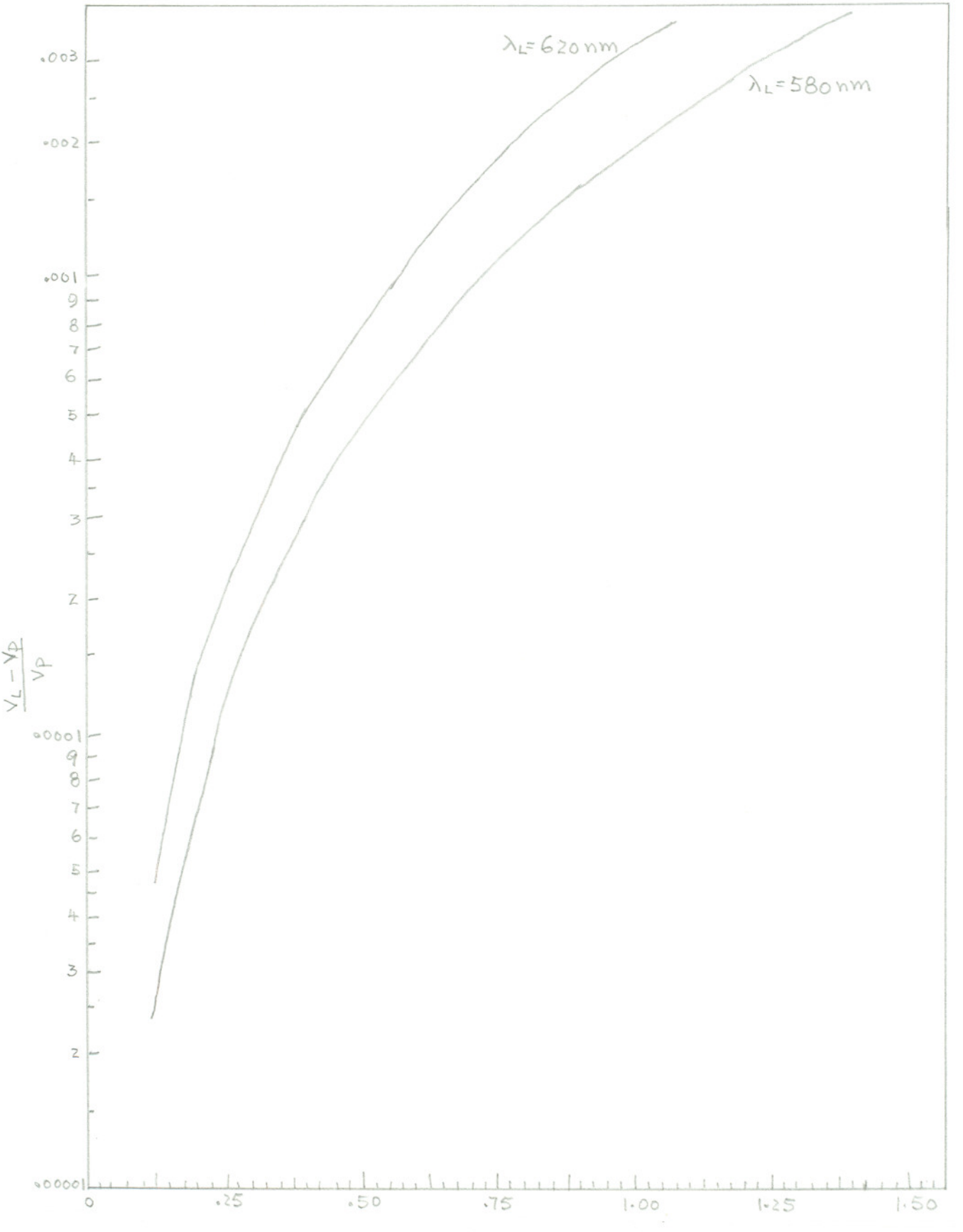

Figure 12 Ratio of 'overlap' vs cell thickness

at 580 nm and 0.3% at 620 nm. A much more important effect is that the pump and laser beams are not in line as they focus into the dye cell, if figure 8a is used. However, if the lasing region is confined within a short cylinder ($l \lesssim 1$ mm) with small cross-sectional area ($\omega_o \sim 0.024$ mm), the 'overlap' discrepancy can be neglected.

When the pump power exceeds the threshold power required, laser light will be generated under favourable conditions. This light will propagate towards the mirror R_1, as shown in figure 8, with the wave front curvature of the propagating light described by eq. 29. From the property of mirrors that a light ray will retrace itself if the light ray is at normal incidence to the mirror surface, and by matching the phase front radius of curvature of dye laser light from the lasing region with a concave spherical mirror the same radius of curvature properly positioned, the beam will refocus onto the same 'spot'.

In this case, a commercially available spherical concave mirror R_1 with radius of curvature of 5 cm, to be positioned about 5 cm from the dye was chosen.

The dye laser beam remerges from the lasing region after refection from R_1 and propagates towards the spherical concave mirror R_2. Since a collimated light beam will emerge if a light source is positioned at the focus of the concave mirror, and since the beam waist in the dye is positioned at the focus of the spherical concave mirror R_2 as

explained earlier from the threshold power density requirement, the dye laser light from R_2 is collimated and directed towards the mirror R_3. The beam size at R_2 is sufficiently large that the wavefront remains essentially plane according to eq. 28 over the whole space between R_2 and R_3. For this reason the astigmatic path difference between R_2 and R_3 due to the Brewster prism (see figure 8) has almost no effect on the resonator mode. From the property of mirrors that a light ray retraces itself if the light ray is at normal incidence to the mirror surface, it is evident that a mirror with radius of curvature nearly infinite will reflect the beam from R_2 onto itself and return it towards the lasing region. This recollimated beam will then focus onto the lasing region after reflected from mirror R_2 for further amplification.

This, then, completes the analysis of the 3-mirror folded resonator.

3.3.3 OUTPUT LINEWIDTH

Through wavelength-selective resonator feedback, a laser may be tuned. The selected output radiation constitutes a spectrum of a certain linewidth. This linewidth will be found to be dependent on the dispersion in the refractive index of the prism and the radius of curvature of the mirror R_3. This situation is illustrated in figure 13.

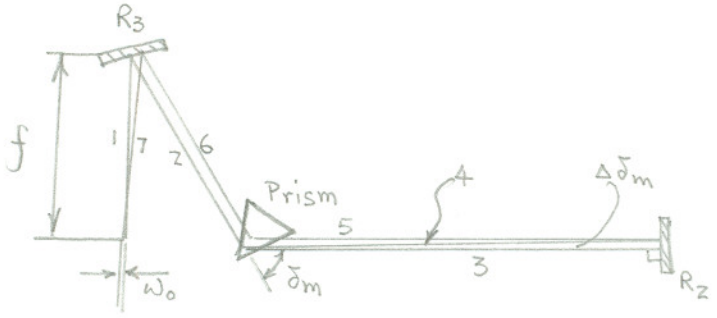

Figure 13 Dispersive property of a prism

Let 1 in figure 13 be the first ray bundle comprising of all the fluorescence emission photons from the centre of the lasing region. This bundle after reflection by the concave mirror R_3 is deviated by a prism P through an angle that depends on the wavelength.

Assume that the refractive index $n(\lambda)$ of the prism can be approximated by a linear equation of the form

$$n(\lambda) = b + a\lambda \qquad 34$$

where a and b are constants, and λ = wavelength (nm).

For example, a SF-4 glass prism has refractive index as

λ (nm)	n
643.8	1.74851
589.3	1.75496
546.1	1.76168
486.1	1.77473

n can be expressed through linear regression analysis as

$$n(\lambda) = 1.85399 - 1.6603 \times 10^{-4} \lambda \qquad 35$$

The equation is as shown in figure 14. The prism's refractive index

of wavelength within this band (486.1 nm to 643.8 nm) can now be estimated by using eq. 35. For example, n(580 nm) = 1.75769.

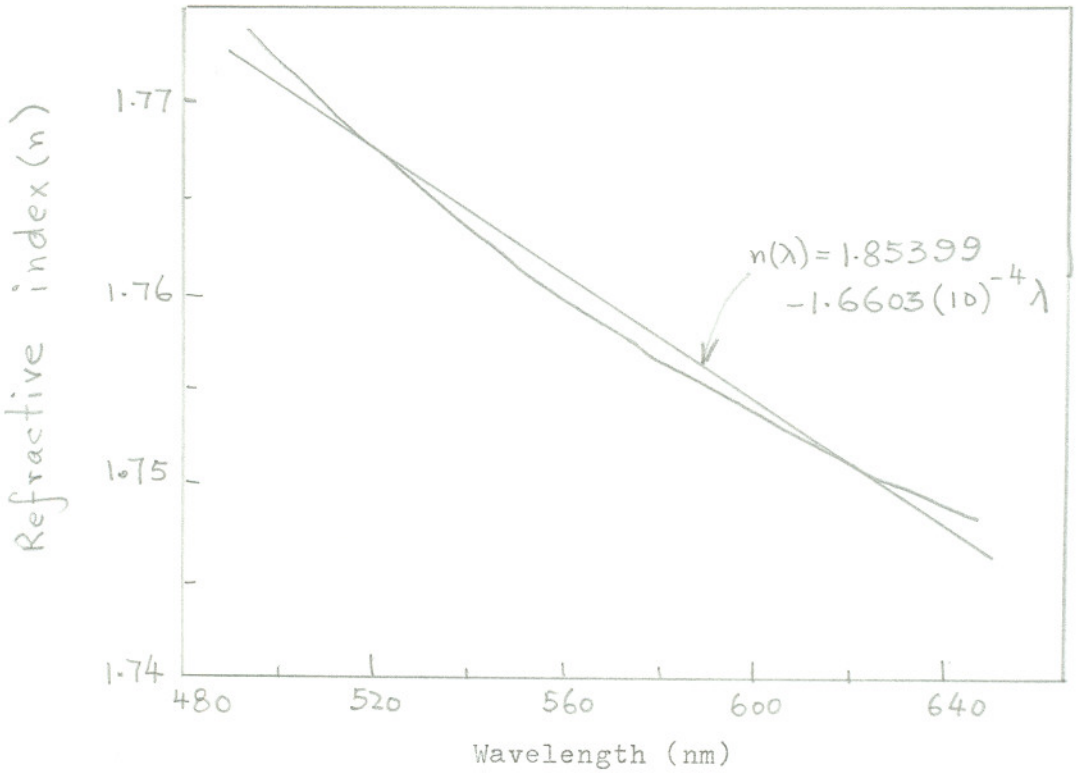

Figure 14 Refractive index of SF-4 glass vs wavelength

The prism's refractive index is related to the minimum angle of deviation by[23]

$$n = \frac{\sin \frac{1}{2}(\alpha + \delta_m)}{\sin \frac{1}{2}\alpha} \qquad 36$$

where α = prism's apex angle,

ϕ = angle of incidence $\sim$ Brewster angle = arctan (n(λ)), and

δ_m = angle of deviation

= angle between the incident ray and emerging ray from the prism as shown in figure 15.

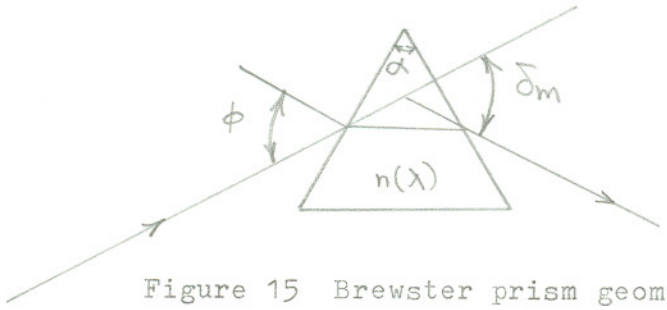

Figure 15 Brewster prism geometry

The minimum angle of deviation can be adjusted by rotating the prism. This is necessary to minimize the surface reflection of dye light from the prism. For example, with $\alpha = 60^\circ$ and n(580nm) = 1.75769, the angle of deviation can be calculated to be 63.0°.

The difference in n due to the difference in λ, implies that δ_m is different for different λ as is obvious from eq. 34 and eq. 36. For a small deviation in Δn due to a wavelength shift, it can be shown from eq. 36 that the perturbed angle of deviation $\Delta\delta_m$ can be found to be

$$\Delta\delta_m = \frac{2 \sin \frac{1}{2}\alpha}{\cos \frac{1}{2}(\alpha + \delta_m)} \Delta n \qquad 37$$

By differentiating eq. 34 with respect to λ, and substituting into eq. 37, $\Delta\delta_m$ can be expressed as a function of difference wavelength $\Delta\lambda$.

$$\Delta\delta_m = \frac{2a \sin \frac{1}{2}\alpha}{\cos \frac{1}{2}(\alpha + \delta_m)} \Delta\lambda \qquad 38$$

Since a plane mirror R_2 can only be positioned normal to a ray

with a particular wavelength, the ray with this wavelength can then retrace itself throughout the resonator. This particular ray defines a resonator axis. 1, 2, 3 in figure 13 form a resonator axis. Another ray 4 with different wavelength ($\lambda + \Delta\lambda$) approaches the plane mirror R_2 at an angle of incidence $\Delta\delta_m$ after passing through the prism. This beam reflected from R_2 as 5 then refracts back through the prism again and is deviated further by $\Delta\delta_m$ emerging as 6. Upon reflection by the mirror R_3, this ray 7 is clearly displaced by a distance $2f \cdot \Delta\delta_m$ at a distance $f = \frac{R_3}{2}$, where R_3 = radius of curvature of mirror R_3, away. Since f is approximately the distance from the mirror R_3 to the dye cell, the deviated ray will fail to pass through the pumped region if the deviation $2f \cdot \Delta\delta_m$ is comparable to the beam spot radius ω_0. By this criterion no oscillation is possible beyond this perturbed angle of deviation, $\Delta\delta_m = \frac{\omega_0}{R_3}$. Since the beam can deviate to either side of the resonator axis, there is a total angle tolerance of $2\Delta\delta_m$. Therefore the output linewidth from eq. 38 can now be estimated to be

$$\Delta\lambda = \frac{\cos\frac{1}{2}(\alpha+\delta_m)}{a \sin\frac{1}{2}\alpha} \frac{\omega_0}{R_3} \qquad 39$$

For a prism with refractive index as a function of λ as in eq. 35, apex angle $\alpha = 60^\circ$, the angle of deviation δ_m calculated to be 63.0° at wavelength $\lambda = 580$ nm, the beam radius $\omega_0 = 0.024$ mm and a mirror radius of curvature $R_3 = 10$ cm, it can be shown by using eq. 39 that $\Delta\lambda = 1.38$ nm.

Since for spectroscopic applications the wavelength values are often expressed in terms of wavenumbers, eq. 39 can be modified to give a linewidth in wavenumber units. Since the product of wavelength λ and wavenumber ν is unity, it can be shown that

$$\Delta\nu = -\frac{\Delta\lambda}{\lambda^2} \qquad 40$$

For example, when $\Delta\lambda$ = 1.38 nm, $|\Delta\nu|$ =41.0 cm^{-1} at λ = 580 nm.

By substituting eq. 40 into eq. 39, the output linewidth in terms of wavenumber is then

$$|\Delta\nu| = \frac{\cos\frac{1}{2}(\alpha+\delta_m)}{a\sin\frac{1}{2}\alpha}\,\frac{\omega_0}{\lambda^2 R_3} \qquad 41$$

3.4 FLOW RATE ANALYSIS

The need for a flowing dye solution is two fold: 1) to decrease triplet state absorption and 2) to remove heat. A high flow rate does not affect the singlet-singlet transition because its decay rate constant k_{31} is substantially higher than the rate at which molecules can be moved through the pumped region of the dye.

As was pointed out in the previous section, the triplet-singlet transition rate constant k_{21} has to reach a certain value before any lasing oscillation can occur. The transition rate constant between two states is the reciprocal of the lifetime of a molecule between the same two states. Thus, it is obvious that if the rate constant

is low, an accumulation of the triplet state would occur, and would quench the laser action. Thus, the removal of the triplet state is necessary and this can be accomplished by 1) triplet quencher, see section 3.1, or 2) by physical removal of the molecules with electrons in the triplet state.

Since the quantitative effect of the triplet quencher on the dye solution was not known, we decided first to investigate the other method of removing the triplet state. For the present case, the minimum k_{21} is 2.8×10^{6} sec.$^{-1}$, which corresponds to a maximum triplet lifetime of 3.57×10^{-7} sec. If the pump beam radius = 0.024 mm, to physically replenish the whole lasing volume in a time corresponding to k_{21}^{-1}, the flow rate has to be greater than 134 m/sec. This obviously is physically very difficult. However, closer examination of the replenishing process, reveals that it is still possible to have a laser operating with decreased efficiency and increased threshold power density requirement using rapid flow without a triplet quencher.

Consider a 'sheet' of dye solution of thickness l, moving at velocity v along the x axis transverse to the pumping beam. Assume that a circular cross-section is uniformly illuminated by the pump beam of radius ω_o, as illustrated in figure 16. This cross-sectional area is inscribed by the equation $x^2 + y^2 = \omega_o^2$.

At time t, the solution has moved a distance of vt. Clearly the section A in figure 16 is the region full of replenished solution.

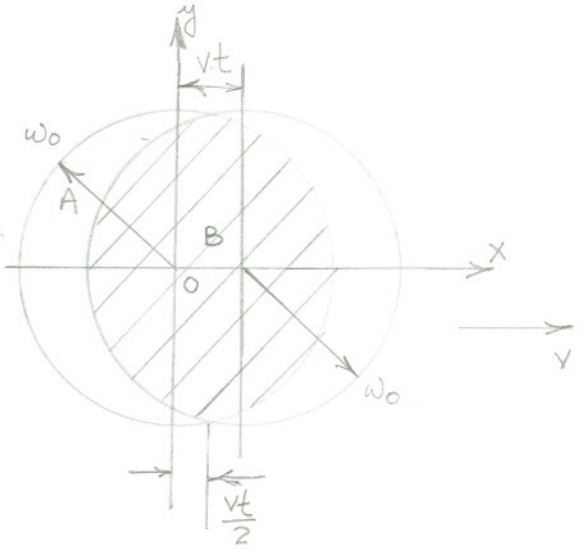

Figure 16 Overlapping area of two identical circles when one is linearly displaced by a constant velocity

This volume can provide maximum dye laser amplification. Assume section B, now filled with molecules excited to the triplet state, provides no gain to the dye laser. Clearly the ratio of area A to the circle area gives the ratio of the useful laser gain volume V_L to the pump beam volume V_p. The area of section B can be calculated as

$$B = \int_{vt-\omega_0}^{\frac{vt}{2}} \int_{-\sqrt{\omega_0^2-(x-vt)^2}}^{\sqrt{\omega_0^2-(x-vt)^2}} dy\,dx + \int_{\frac{vt}{2}}^{\omega_0} \int_{-\sqrt{\omega_0^2-x^2}}^{\sqrt{\omega_0^2-x^2}} dy\,dx$$

$$= \omega_0^2 \left[\pi - 2\sin^{-1}\left(\frac{vt}{2\omega_0}\right) - \frac{vt}{2\omega_0}\sqrt{1-\left(\frac{vt}{2\omega_0}\right)^2} \right] \qquad 42$$

By using eq. 42, the ratio V_L / V_p can be derived as

$$\frac{V_L}{V_p} = \frac{A}{\pi\omega_0^2} = \frac{\pi\omega_0^2 - B}{\pi\omega_0^2}$$

$$= \frac{1}{\pi}\left[2\sin^{-1}\left(\frac{vt}{2\omega_0}\right) + \frac{vt}{2\omega_0}\sqrt{1-\left(\frac{vt}{2\omega_0}\right)^2} \right] \qquad 43$$

The ratio V_L / V_P is plotted as a function of the ratio t / t_r in figure 17. The residence time t_r is defined as the total time needed for a dye molecule to pass through the middle of the pump beam, i.e. $t_r = \frac{2\omega_o}{v}$. Clearly, the ratio is a good approximation only if the 'sheet' thickness is significantly less than 1 mm for reasons discussed in section 3.3.2 and shown in figure 12.

It is also evident that if the singlet-triplet crossing time τ_{st} ($1 / k_{32}$) is less than t_r, the principal means of reducing triplet absorption is by replenishing the dye lasing volume with fresh solution during the time τ_{st}. It is clear that for a velocity v, the fractional beam area giving amplification is the same as the ratio $t_f = \tau_{st} / t_r$. Either by eq. 46 or from figure 17 with t_f, the ratio V_L / V_P can be found. With this ratio, the new minimum threshold power density can be estimated as $\frac{1.12}{\frac{V_L}{V_P}}$ kW/cm^2, where 1.12 kW/cm^2 is the minimum threshold power density obtained in section 3.2. The new dye laser efficiency can also similarly calculated as $\frac{V_L}{V_P} \cdot \eta$.

For example, velocity of dye solution $\sim$ 7 m/sec. and beam radius = 0.024 mm, $t_r = 6.8 \times 10^{-6}$ sec. and $\tau_{st} = 3 \times 10^{-7}$ sec. (ref. 24), V_L / V_P is then 0.042. The new minimum threshold power density is therefore about 27 kW/cm^2, which is still below the expected available pump power density of 34.9 kW/cm^2 calculated in section 3.3.2. If the velocity of dye solution is increased to 14 m/sec., the corresponding threshold would be about 13.4 kW/cm^2.

Figure 17 Ratio $\frac{V_L}{V_P}$ vs fractional residence time

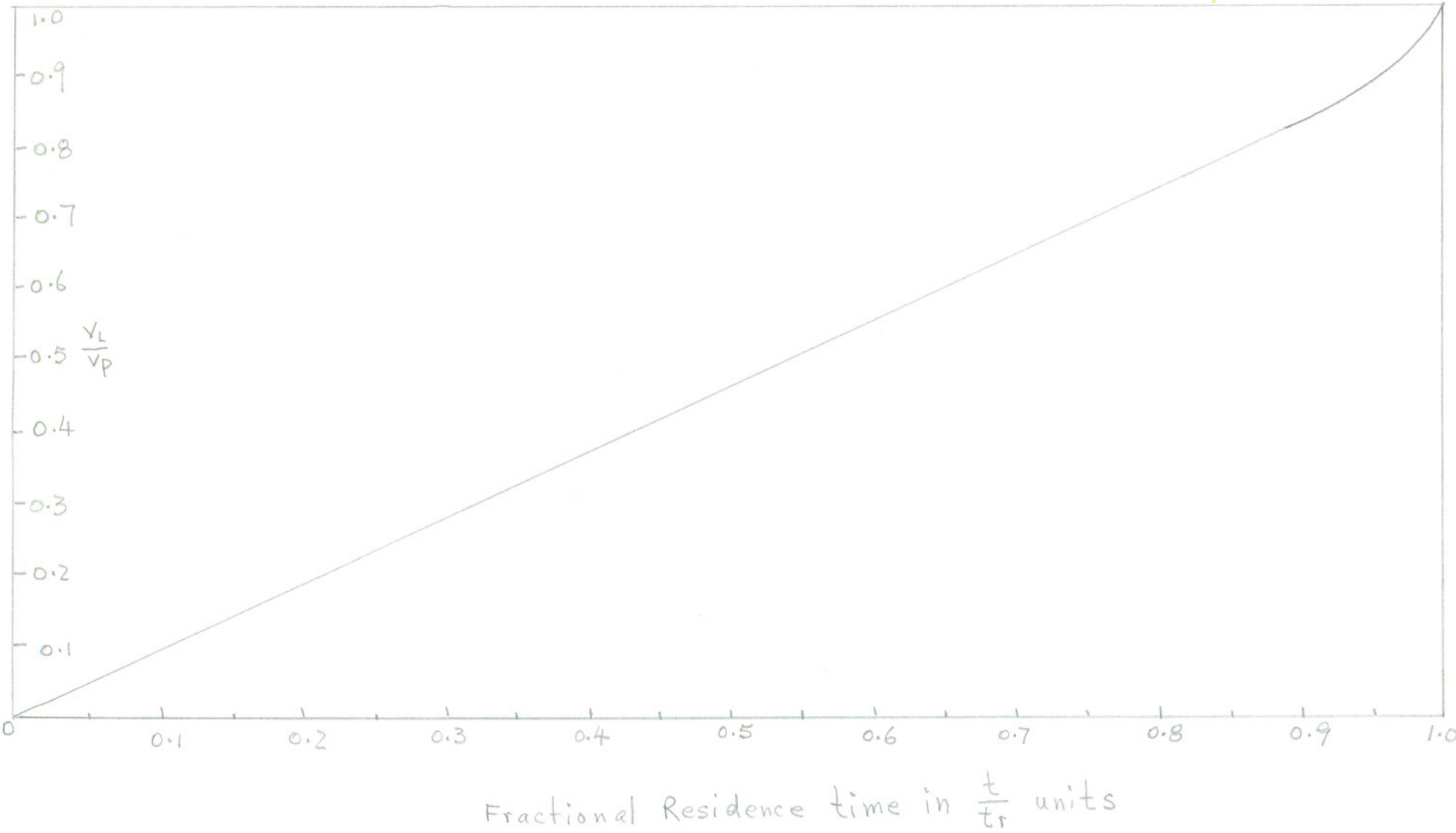

This shows the importance of having a high flow rate as it decreases the threshold power density requirement.

Aside from increasing laser efficiency, high flow rate is needed to remove the heat introduced by the pumping laser. If the pump power is adjusted to 1.5 watt, and the dye laser is operating at 30% conversion efficiency, 450 mW dye laser output is available. And a substantial portion of the remaining energy 1.05 watt is dissipated into heating the solvent. Since a substantial amount of power is dissipated into a small cylindrical volume (ω_o = 0.024 mm, l = 1 mm), this heating effect must be investigated.

Consider a differential lasing region of thickness l made up of dye solution of density ρ and specific heat s, moving at a linear velocity v along y axis transverse to the Gaussian distributed pumping beam of beam radius ω_o with fractional power W dissipated as heating the solution, it can be shown that the total rise in temperature ΔT for the differential region assuming no heat is conducted to the surrounding can be expressed as

$$\Delta T = \int_{-\infty}^{\infty} \frac{W}{\pi \omega_o^2} \frac{1}{\rho s l v} e^{-\frac{x^2}{\omega_o^2} - \frac{y^2}{\omega_o^2}} dy$$

$$= \frac{W}{\sqrt{\pi}\, \omega_o \rho s l v} e^{-\frac{y^2}{\omega_o^2}} \qquad 44$$

For example, if 1 watt is dissipated as heat by the pumping beam of beam radius ω_o = 0.024 mm, and the lasing volume is made up of l = ¼ mm thick ethylene glycol sheet of density ρ = 1.112 gm/cm^3 and

specific heat s = 1.53 Joules/gm ^{o}C moving at a velocity v = 700 cm/sec., ΔT can be calculated by employing eq. 44 to be 7.89 ^{o}C. And if the same 1 watt is dissipated as heat by the pumping beam of beam radius ω_o = 0.024 mm and the lasing volume is made up of l = 1 mm thick ethanol of density ρ = 0.81 gm/cm^3, and specific heat s = 2.51 Joules/gm ^{o}C moving at a velocity v = 14 m/sec., ΔT can be calculated by using eq. 44 to be 0.83 ^{o}C.

Eq. 44 clearly overestimates the temperature increase because the heat conduction to the surrounding dye solution is neglected. However, the functional dependence of temperature increase is evident. To avoid the dye laser output lineshift due to dye molecule temperature fluctuation, it is necessary to have a large cross-sectional area $\pi\omega_o^2$, but this is impossible because a high pump power density is required. Similarly because of the wave propagation within the resonator, the thickness l has to be small. Finally the solubility and viscosity of the dye solution for use with the particular dye cell design has to be considered. By these constraints, once a solvent is chosen, both the specific heat and density are determined. Therefore the only alternative to lower the total temperature increase is to have a high flow rate.

Further heating of the dye solvent is produced by the mechanical pump used to circulate the solution. To remove the heat, the dye was circulated through a reservoir placed in an ice bath.

To achieve a high flow rate to increase the dye laser efficiency and decrease the heating problem, a heavy-duty magnetic coupled pump was used in this experiment. The magnetic coupled pump was chosen to avoid grease contamination which would result if other type of pumps were used. Grease in the dye solution would cause a decrease in the fluorescence efficiency of the dye.

4.0 MECHANICAL CONSIDERATIONS

From the previous section, the physical dimensions of the lasing volume with a flowing dye solution are specified. This section discusses the two possible ways to accomplish these goals: 1) confined flow in a cell, and 2) open 'sheet' flow from a nozzle. The sheet of flowing dye solution has to form an optically uniform window with minimum diffraction and scattering losses.

The idea of constructing an enclosed cell is appealing, since the optical quality of the sheet is defined by the windows and low viscosity dye solvents can be used. The cell windows, however, are frequently damaged by pump light when dye solution is circulated through the cell and irradiated. It is believed that the pump beam disintegrates the slower moving dye molecules at the interface between the solvent and the window, thus damaging or 'burning' the windows.

An operating cell was constructed as shown in figure 18. The

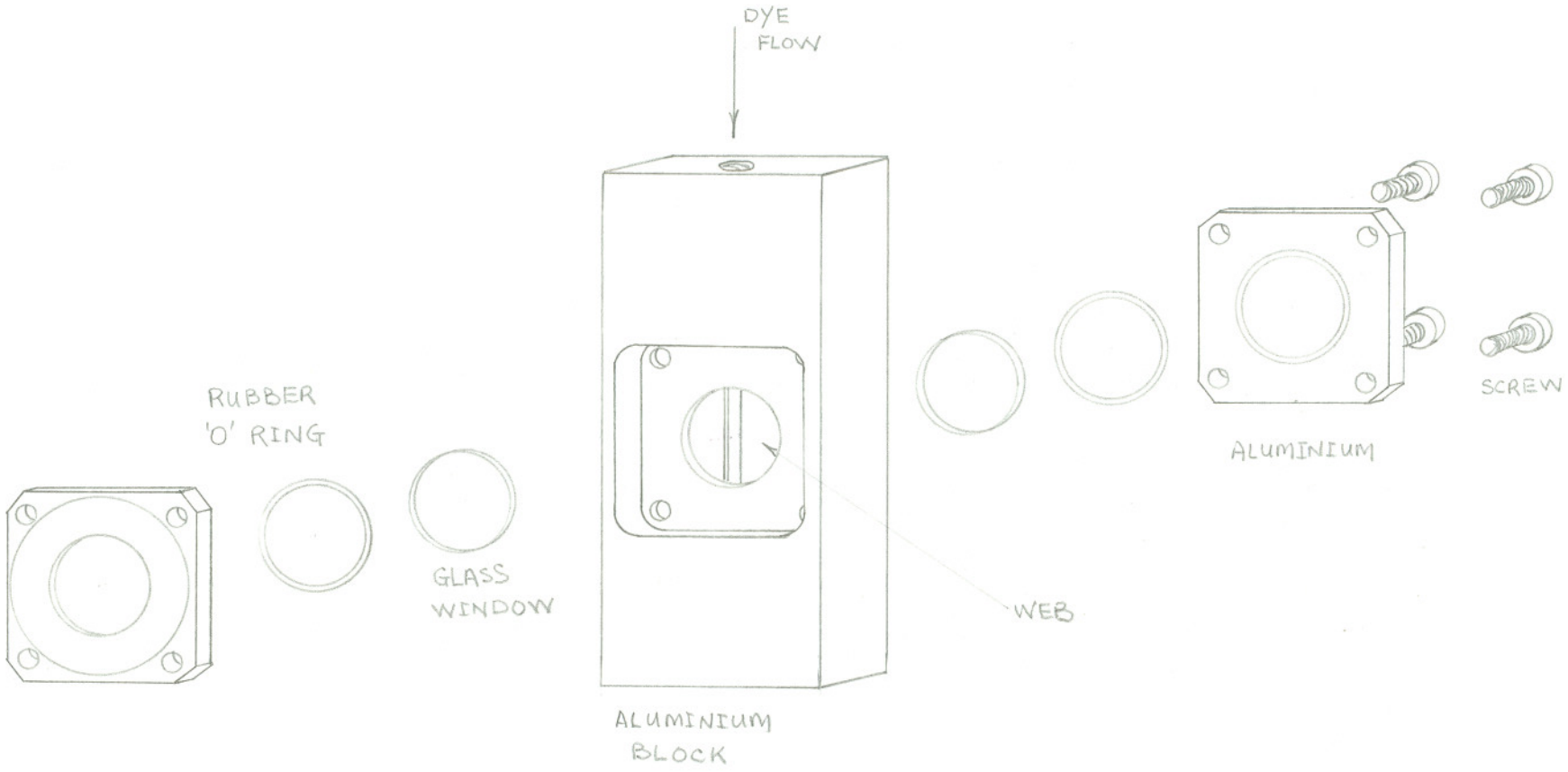

Figure 18 Explored view of the dye cell

thickness of the web is about 1 mm. Ethyl alcohol was used as solvent because it has a low viscosity, thus permitting a high flow rate. The flow rate at the window was measured to be 14 m/sec.

The dye jet construction has the advantage that there are no windows to burn, therefore permitting more reliable operation and higher intensities. But the liquid jet is subject to problems of poor optical quality surfaces due to surface ripples in the flowing sheet and bubbles arising from agitation of the projected solvent on contact with the receiver of the liquid. However, these bubbles do introduce oxygen into the liquid and serve as a triplet quencher. These factors can be minimized by careful design and construction.

It is known that in order to obtain a smooth 'sheet' with minimum ripples, it is necessary to have a flow with low Reynolds number. Reynolds number R is defined as[25]

$$R = \frac{\rho v d}{\eta} \qquad 45$$

where ρ = density of fluid,

v = velocity of fluid,

d = thickness of the flowing 'sheet', and

η = viscosity of fluid.

Reynolds number is a measure of turbulence. A smooth flow can usually be achieved if $30 < R < 200$. It is obvious that once a viscous liquid is chosen for its particular property, e.g. solubility, the density and viscosity are fixed. For the present case, ethylene

glycol is chosen because it has a high viscosity (20 cP) and the dye can be dissolved to the necessary concentration. The factors that can lower the Reynolds number are a decrease in velocity and a decrease in the 'sheet' thickness. But the velocity has to be high for high efficiency and low threshold power density, therefore the only means is a decrease in the 'sheet' thickness.

For example, the density, velocity and viscosity of a 0.25 mm thick ethylene glycol sheet are 1.11 gm/cm^3, 7 m/sec. and 20 cP respectively; Reynolds number can be calculated by using eq. 45 to be about 97.1. Therefore, if a nozzle has these specifications and flow rate, a smooth sheet flow can be expected. A successful nozzle was constructed after considerable experimentation, and is shown in figure 19.

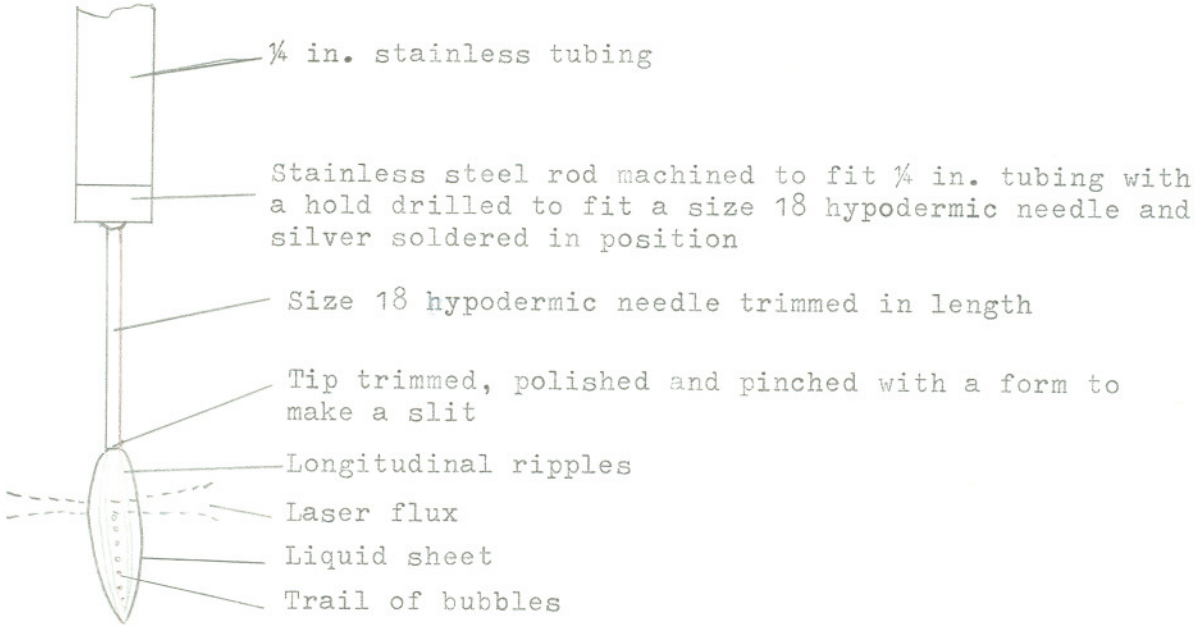

Figure 19 Nozzle

The 'flowing sheet' from the working nozzle still had longitudinal ripples as shown in figure 19. It is suspected that these ripples are caused by the uneven nozzle tip surface. These ripples did not cause any serious problem because only a small region (beam radius $\sim$ 0.024 mm) had to be smooth.

5.0 EXPERIMENT

The previous sections discussed the possibility of success in constructing a dye laser. This section describes the experiments on the dye laser so constructed.

The optical arrangement of the equipment was as shown in figure 8. The mirrors and prism were mounted in respective optical holders attached to a steel surface plate by means of magnetic bases. The cell or nozzle was held by a rigid fixture mounted on a magnetic base.

The dye used was Rhodamine 6G and the liquid flow diagram is shown in figure 20. It was necessary to stabilize the liquid temperature through an ice bath in order to obtain a stable dye laser mode. No bubble filtering was used in this prototype design, because it was believed that even if bubbles were present, an intermittant emission of dye laser flux would still be observed.

The dye cell was employed first. In this configuration, the

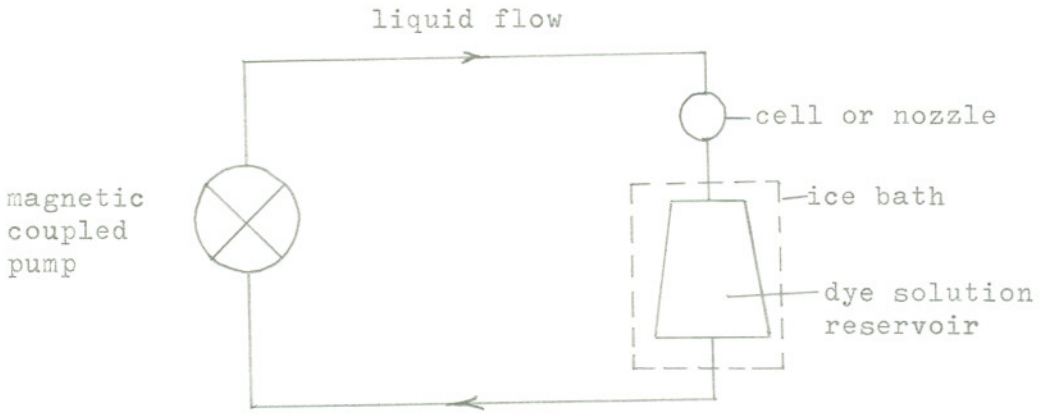

Figure 20 Liquid flow diagram

dye laser was made to operate only when a chopper wheel was used to reduce the window burning problem. The use of the dye cell was abandoned and the dye jet use instead after it was found that the dye/ethyl alcohol solution reacts chemically with the aluminum cell.

During the course of experiments, it was found that the dye solution degraded rapidly with time. The fluorescence of the dye solution was substantially weaker when compared to freshly prepared solution. It is suspected that dimerisation of dye molecules had occurred[26,27].

5.1 RESONATOR ALIGNMENT PROCEDURE

With the astigmatic compensated resonators shown in figure 8, certain alignment procedures were developed, as follows.

For the resonator of figure 8b:

a) The argon ion laser was adjusted to maximum power output at 514.5 nm.

b) The prism was positioned at minimum deviation using the argon beam or the dye fluorescence as the alignment light source.

c) The mirror R_3 was oriented at the proper compensated angle for the dye cell or jet.

d) The mirror R_2 was situated roughly in position.

e) The cell or jet was placed at the Brewster angle (minimum surface reflection) and a sharp spectrum or "rainbow" was formed on the laboratory wall from the fluorescence reflected by the mirror R_3, passing through the prism and reflecting from the mirror R_2.

f) R_1 was then oriented to form another sharp "rainbow" superimposed on the spectrum formed in step e.

g) The "rainbows" were then reflected back into the prism by adjusting R_2. Laser oscillation generally would begin when the adjustments were properly made.

The procedures for aligning the figure 8a configuration were identical to the above except the sequence of steps was then a, c, d, e, b, f, g.

5.2 OUTPUT COUPLING METHOD AND LASER PERFORMANCE

Lasing was observed when all the mirrors used were 100% reflective. When a 5% transmittance mirror was used as an output coupler instead of the 100% reflectance mirror R_2, no lasing was observed. This indicates

that the double-pass excess gain of the dye laser was less than 5%.

When a microscope glass slide or a cover glass was inserted in the dye laser beam at the Brewster angle, some light could be coupled out of the resonator without quenching the oscillation. The percentage of output coupling was varied through a small range by tilting the slide close to Brewster angle.

With the glass slide coupling, and a 1.5 watt pump power, a maximum dye laser power output of about 40 mW at 580 nm was observed. This corresponds to an efficiency of 2.67%.

The power output fluctuated during the entire operating period. It is believed that this is due to the bubbles formed by vaporized dye solution by the pump beam.

As estimated tuning range from 570 nm to 610 nm was observed with no output coupling. When a glass plate output coupler was used, the tunability was as expected, substantially decreased, due to the higher threshold.

A spectrum of the laser was recorded using a 1-meter Jarrell-Ash spectrometer with the glass slide coupler. As shown in figure 21 with the wavelength set at about 17377 cm^{-1} (575 nm), the oscillation occupied a 22 cm^{-1} (0.73 nm) bandwidth made up of about six lines each of about 2 cm^{-1} (0.066 nm) in width. The maximum amplitudes of

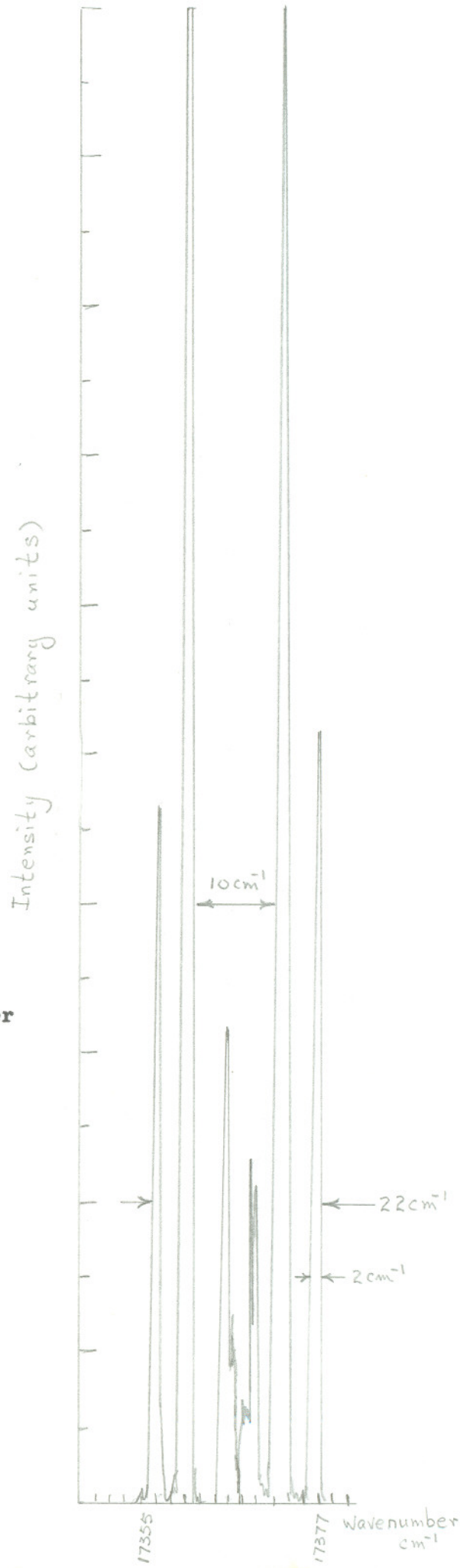

Figure 21 Spectrograph of dye laser output at about 575 nm

the six lines are equally spaced at about 4 cm^{-1} (0.132 nm). By the symmetric pattern, it can be seen that the spacing between maximum and minimum is about 2 cm^{-1} (0.066 nm).

The 22 cm^{-1} bandwidth is about half the calculated bandwidth of 41.0 cm^{-1} (1.38 nm) in section 3.3.3, but this is to be expected because the theorectical calculation assumes that oscillation is quenched only when the misalignment per pass is as great as the beam diameter in the dye cell, and amplification is constant throughout the lasing region.

The individual lines in the output spectrum existed because resonances occur in the glass slide used as the output coupler. It can be shown by considering either maximum or minimum surface reflection within the glass slide that[28]

$$\Delta \nu \simeq \frac{1}{2nd\cos\phi} \qquad 46$$

$$\Delta \lambda \simeq \frac{\lambda^2}{2nd\cos\phi} \qquad 47$$

where $\Delta\nu$ = linewidth in wavenumber (cm^{-1}),

n = refractive index of glass slide $\sim$ 1.53,

d = thickness of glass slide $\sim$ 1 mm,

ϕ = angle of reflectance,

$\Delta\lambda$ = linewidth in wavelength (nm), and

λ = wavelength of emitting laser light.

With the angle of incidence $\sim$ Brewster angle = arctan(n), it

can be calculated that the spacing between the lines due to the glass plate $\Delta\omega$ = 3.90 cm^{-1} (0.09 nm). The measured spacing between lines of 4 cm^{-1} (0.132 nm) is in close approximation with the calculated 3.90 cm^{-1}.

By symmetry property, it can be deduced that the wavelength difference between minimum and maximum intensity is about half the wavelength difference in the line spacing, or about 1.95 cm^{-1} (0.0645 nm). This is in close accordance with the experimental result of 2 cm^{-1} (0.066 nm).

5.3 RAMAN SPECTROGRAPH OF CARBON TETRACHLORIDE

During the course of experiment, the Raman spectrum of carbon tetrachloride excited with 579 nm light from the dye laser was recorded as shown in figure 22. Since the peaks of the Raman lines are $\sim$ 30 cm^{-1} wide and the dye laser spectrum is 22 cm^{-1} wide, its spectral purity is therefore sufficient for Raman scattering experiments.

6.0 CONCLUSION

A successful dye laser has been constructed as predicted by the theory. It had also been shown that the laser has a 'wide' continuous tuning range.

Figure 22 **Spectrograph of Carbon Tetrachloride**

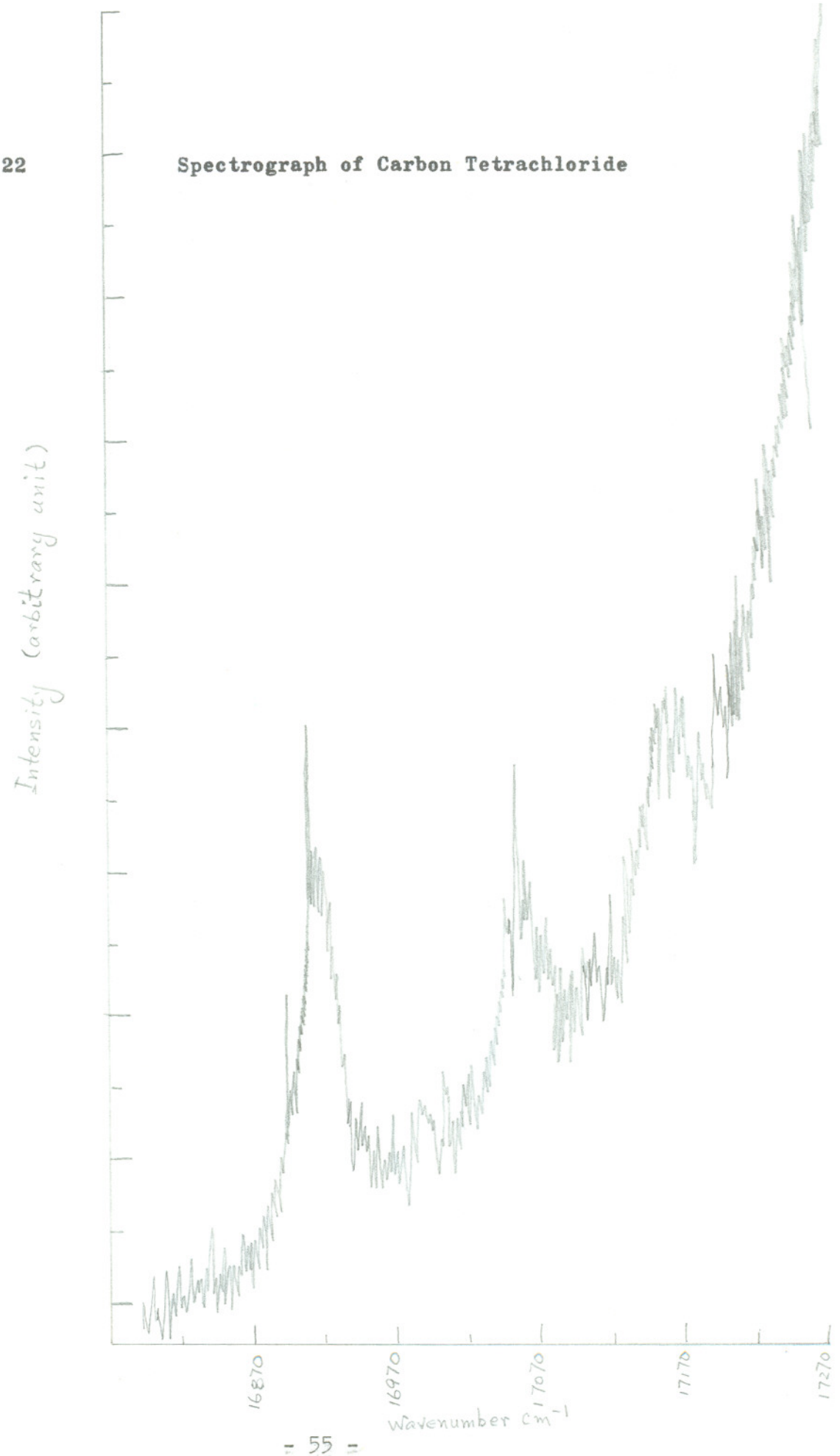

Although its tunability makes the dye laser extremely versatile, its overall efficiency is still very low in continuous operation, because it depends upon another CW laser with efficiency below 0.1% for its excitation. This inefficiency might be overcome with some type of direct electrical pumping of the dye, possibly through electrochemiluminescence as proposed by Measures[29]. So far no successful laser operation has been reported using that scheme.

The flow rate might be increased to control the triplet lifetime if dye vapor is used instead of liquid - since it might be easier to circulate gas than liquid at very high velocities. Recently a successful pulse mode laser using dye vapor has been reported by Smith, et al[30]. This certainly deserves intensive research.

7.0 REFERENCES

1. P.Sorokin, "Organic Lasers", Sci.Am. (February 1969) pp.30-40

2. M.J.Weber and M.Bass, "Frequency and Time Dependent Gain Characteristics of Dye Lasers", IEEE J. Quantum Electron. QE-5 (April 1969) pp.175-188

3. R.Pappalardo,H.Samelson, and A.Lempicki, "Long-Pulse Laser Emission form Rhodamine 6G", IEEE J. Quantum Electron. QE-6 (November 1970) pp.716-725

4. B.B.Snavely and O.G.Peterson, "Experimental Measurement of the Critical Population Inversion for the Dye Solution Laser", IEEE J. Quantum Electron. QE-4 (October 1968) pp. 540-545

5. P.P.Sorokin, J.R.Lankard, V.L.Moruzzi, and E.C.Hammond, "Flashlamp-pumped Organic Dye Lasers", J.Chem.Phys. Vol.48, No.10 (May 1968) pp. 4726-4714

6. P.P.Sorokin, J.R.Lankard, E.C.Hammond, and V.L.Moruzzi, "Laser-Pumped Stimulated Emission form Organic Dyes: Experimental Studies and Analytical Comparisons", IBM J.Res.Dev. 11 (March 1967) pp.130-148

7. B.H.Soffer and B.B.McFarland, "Continuously Tunable, Narrow-Band Organic Dye Lasers", Appl.Phys.Lett. Vol.10, No.10 (May 1967) pp.266-267

8. O.G.Peterson, S.A.Tuccio, and B.B.Snavely, "CW Operation of an Organic Dye Solution Laser", Appl.Phys.Lett. Vol.11, No.6 (September 1970) pp.245-247

9. L.P.Letouzey and S.O.Sari, "Continuously Pulse Train Dye Laser Using an Open Flowing Passive Absorber", Appl.Phys.Lett. Vol.23, No.6 (September 1973) pp.311-313

10. P.K.Runge and R.Rosenberg, "Unconfined Flowing-Dye Films for CW Dye Lasers", IEEE J. Quantum Electron. QE-8 (December 1972)

11. B.Wellegehausen, H.Welling and R.Beigang, "A Narrowband Jet Stream Dye Laser", Appl.Phys.3 (May 1974) pp.387-391

12. J.M. Yarborough, "CW Dye Laser Emission Spanning the Visible Spectrum", Appl.Phys.Lett. Vol.24, No.12 (June 1974) pp.629-630

13. B.B. Snavely, "Flashlamp-Excited Organic Dye Lasers", Proc. IEEE 57, (August 1969) pp.1374-1390

14. A.Dienes, E.P.Ippen, and C.V.Shank, "High-Efficiency Tunable CW Dye Laser", IEEE J. Quantum Electron. QE-8 (March 1972) pp.388

15. R.R.Jacobs, H.Samelson, and A.Lempicki, "Losses in CW Dye Lasers", J.Appl.Phys. Vol.44 (January 1973) pp.263-272

16. N.J.Turro, Molecular Photochemistry, New York:Benjamin, 1965, pp.54-55

17. B.I.Stepanov and A.N.Rubinov, "Lasers Based on Solutions of Organic Dyes", Sov.Phys.Usp.11 (November 1968) pp.304-319

18. G.A.Massey and A.E.Siegman, "Reflection and Refraction of Gaussian Light Beams at Tilted Ellipsoidal Surfaces", Appl.Opt. Vol.8, (May 1969) pp.975-978

19. J.M.Telle and C.L.Tang, "New Method for Electro-Optical Tuning of Tunable Lasers", Appl.Phys.Lett. Vol.24, No.2, (January 1974) pp.85-87

20. F.A.Jenkins and H.E.White, Foundamentals of Optics, New York: McGraw-Hill, 1957, pp.95

21. H.Kogelnik and T.Li, "Laser Beams and Resonators", Appl.Opt. Vol.5 (October 1966) pp.1550-1567

22. A.E.Siegman, An Introduction to Lasers and Masers, McGraw-Hill, 1971, Ch.8

23. same as ref.20, pp.22

24. J.P.Webb, W.C.McColgin, and O.G.Peterson, "Intersystem Crossing Rate and Triplet State Lifetime for a Lasing Dye", J.Chem.Phys. Vol.53, No.11 (December 1970) pp.4227-4229

25. Landau and Lifshitz, Fluid Mechanics, Pergamon Press Ltd., 1959, pp.63

26. D.Kato and A.Sugimura, "Deterioration of Rhodamine 6G Dye Solution in Methanol", Opt.Comm. Vol.10 (April 1974) pp.327-330

27. K.K.Rohatgi and G.S.Singhal, "Nature of Bonding in Dye Aggregates", J.Appl.Chem. Vol.70, No.6 (June 1966) pp.1695-1701

28. same as ref.20, pp.282

29. R.M. Measures, "Prospects for Developing a Laser Based on Electrochemiluminescence", Appl.Opt. Vol.13 (May 1974) pp.1121-1133

30. P.W.Smith, P.F.Liao, C.V.Shank, T.K.Gustafson, C.Lin and P.J. Maloney, "Optically Excited Organic Dye Vapour Laser", Appl.Phys. Lett. Vol.25, No.3 (August 1974) pp.144-146